Origin of a crustal splay fault and its relation to the seismogenic zone and underplating at the erosional north Ecuador–south Colombia oceanic margin

J.-Y. Collot,[1] W. Agudelo,[1] A. Ribodetti,[1] and B. Marcaillou[2]

[1]   Splay faults within accretionary complexes are commonly associated with the updip limit of the seismogenic zone. Prestack depth migration of a multichannel seismic line across the north Ecuador–south Colombia oceanic margin images a crustal splay fault that correlates with the seaward limit of the rupture zone of the 1958 (Mw 7.7) tsunamogenic subduction earthquake. The splay fault separates 5–6.6 km/s velocity, inner wedge basement rocks, which belong to the accreted Gorgona oceanic terrane, from 4 to 5 km/s velocity outer wedge rocks. The outer wedge is dominated by basal tectonic erosion. Despite a 3-km-thick trench fill, subduction of 2-km-high seamount prevented tectonic accretion and promotes basal tectonic erosion. The low-velocity and poorly reflective subduction channel that underlies the outer wedge is associated with the aseismic, décollement thrust. Subduction channel fluids are expected to migrate upward along splay faults and alter outer wedge rocks. Conversely, duplexes are interpreted to form from and above subducting sediment, at ∼14- to 15-km depths between the overlapping seismogenic part of the splay fault and the underlying aseismic décollement. Coeval basal erosion of the outer wedge and underplating beneath the apex of inner wedge control the margin mass budget, which comes out negative. Intraoceanic basement fossil listric normal faults and a rift zone inverted in a flower structure reflect the evolution of the Gorgona terrane from Cretaceous extension to likely Eocene oblique compression. The splay faults could have resulted from tectonic inversion of listric normal faults, thus showing how inherited structures may promote fluid flow across margin basement and control seismogenesis.

1. Introduction

[2]   At subduction trenches, seismic reflection data have revealed seaward verging crustal faults that branch upward and splay away from the plate interface at a ∼10-km depth [*Park et al.*, 2002a]. Such crustal splay faults are out-of-sequence thrust-type faults that break through the upper plate and contribute to significant deformation and thickening of the margin. The importance of these faults has been brought to attention as they may define the updip limit of the rupture zone of some great subduction earthquakes, and contribute to tsunamis generation [*Plafker*, 1972; *Fukao*, 1979; *Kato*, 1983; *Park et al.*, 2000, 2002a; *Cummins and Kaneda*, 2000]. In the Nankai region, splay faults have been suggested to root above an underplated complex, near the

updip limit of the seismogenic zone [*Kitamura et al.*, 2005; *Kimura et al.*, 2007; *Moore et al.*, 2007], where ∼150°C dehydration temperature [*Hyndman and Wang*, 1995; *Hyndman et al.*, 1995] favors diagenetic to low-grade metamorphic reactions, and causes the onset of seismicity [*Moore and Saffer*, 2001; *Saffer and Marone*, 2003]. The geological origin of the splay fault and the nature of the rocks it traverses have important implications on its geometry, mechanics and ability to propagate the coseismic slip rupture and generate tsunamis. Conceptually, a splay fault could break through an accretionary wedge, or reactivate a preexisting fault within or between an igneous backstop and an accretionary wedge, or a suture zone between formerly accreted terranes. In the absence of direct fault sampling, modeling the geometry, origin, and physical properties of the fault and adjacent rock bodies can be achieved from seismic data through the process of prestack depth migration. The resulting seismic image and velocity model help discriminating between various splay faults geological environments but also identifying inherited fault systems, which may be potential candidate for future seismic reactivation. Information of multichannel seismic reflection (MCS) and

---

[1]Geoscience Azur, Université de Nice-Sophia Antipolis, IRD, Université Pierre et Marie Curie, Observatoire de la Côte d'Azur, CNRS, Villefranche-sur-Mer, France.
[2]IFREE/JAMSTEC, Yokosuka, Japan.

wide-angle seismic refraction (WA) data was combined along a geophysical transect (Figure 1) to better display a crustal splay fault and associated plate boundary structures that were identified in the north Ecuador–south Colombia convergent margin [*Collot et al.*, 2004], where great tsunamogenic, subduction earthquakes have occurred during the 20th century [*Kanamori and McNally*, 1982]. In this paper, we analyze the transect detail structures near latitudes 1°30′–1°50′N. We focus on the nature and structure of the margin inner and outer wedges, the subduction channel and the splay fault, as well as on their potential mechanical behavior during the earthquake cycle. We further suggest a structural origin for the splay fault and show how inherited margin structures may affect the present-day and future underplating, basal erosion, rock alteration, and seismogenesis of the margin.

2. Geological Background and Data Collection

[3] The north Ecuador–south Colombia convergent margin comprises mafic, ultramafic, and volcaniclastic basement rocks as indicated by onshore geology [*Goosens and Rose*, 1973; *Gansser*, 1973; *Lebras et al.*, 1987; *Reynaud et al.*, 1999], a narrow frontal wedge in the south (Figure 1) [*Collot et al.*, 2006], and a 30-km-wide accretionary wedge in the north [*Mountney and Westbrook*, 1997; *Marcaillou*, 2003]. The complex structures of this basement resulted from the sequential dextral oblique accretion of allochthonous Cretaceous oceanic terranes [*Reynaud et al.*, 1999; *Cediel et al.*, 2003; *Luzieux et al.*, 2006] including (1) the Dagua terrane in the western Cordillera of Colombia, (2) the Piñon and San Lorenzo terranes in Ecuador [*Reynaud et al.*, 1999], and (3) the Gorgona terrane in Colombia (Figure 2). These terranes accreted during (1) the late Cretaceous–early Eocene [*Cediel et al.*, 2003], (2) the late Campanian [*Luzieux et al.*, 2006] or the Paleocene–late Eocene [*Jaillard et al.*, 1997] and (3) during the Eocene to early Miocene [*Kerr*, 2005; *Cediel et al.*, 2003], respectively. The resulting patchwork of terranes consists of fragments of Pacific oceanic plateaus, volcanic ridges, intraoceanic island arcs, and ophiolites. The Gorgona terrane, which is the site of our geophysical transect (Figure 2), has poorly constrained boundaries because it lies mostly offshore. On the basis of MCS data, *McGeary and Ben-Avraham* [1986] place the terrane landward boundary between the outer shelf Gorgona basement and the inner shelf fore-arc basin. However, the Buenaventura fault that is dextral transpressive is interpreted as the suture trace between the Gorgona and Dagua terranes [*Cediel et al.*, 2003].

[4] The margin is underthrust by the young (<25 Ma [*Hardy*, 1991]) and morphologically complex Nazca plate [*Lonsdale and Klitgord*, 1978] at 5.4 cm/a in an eastward direction (Figure 1) [*Trenkamp et al.*, 2002]. In the study area (Figure 1), the trench contains the Esmeraldas deep-sea turbidite system that is fed by the Esmeraldas canyon [*Collot et al.*, 2005]. The Carnegie Ridge, a major 2-km-high east–west trending volcanic ridge [*Lonsdale*, 1978] enters subduction in central Ecuador. Immediately north of the Carnegie Ridge-trench intersection, the segment of the plate boundary that trends NNE and extends over ∼500 km to Buenaventura was ruptured in 1906 (Figure 1 insert) by a single great thrust event of Mw8.8 [*Kelleher*, 1972;

Kanamori and Given, 1981; *Kanamori and McNally*, 1982]. Three smaller events, adjacent to one another, reactivated part of the 1906 rupture zone from south to north in 1942 (Mw7.8), 1958 (Mw7.7) and 1979 (Mw8.2) [*Mendoza and Dewey*, 1984; *Beck and Ruff*, 1984; *Swenson and Beck*, 1996]. On the basis of the after shocks distribution [*Mendoza and Dewey*, 1984] and modeling spatial variation in earthquake moment release, *Beck and Ruff* [1984] showed that the seaward propagation of the 1958 earthquake brittle rupture zone stopped ∼25 km from the trench, whereas the adjacent 1942 and 1979 earthquake rupture zones extended up to the trench (Figure 1) [*Kanamori and McNally*, 1982; *Mendoza and Dewey*, 1984; *Beck and Ruff*, 1984]. Line SIS-44 was intended to explore the margin structures across the 1958 (Mw 7.7) earthquake rupture zone (Figure 1).

3. Geophysical Data

[5] MCS data were acquired along line SIS-44 with a 4.5-km-long hydrophone streamer and a 48-L air gun source array, and wide-angle seismic data were collected along coincident line SAL06 [*Gailler et al.*, 2007] using ocean bottom hydrophones and ocean bottom seismometers, and a 96-L air gun source (Figure 1). Using bathymetry and the time-migrated seismic section SIS-44, *Collot et al.* [2004] showed that the seaward limit of the 1958 earthquake rupture zone could be associated with a fault-bounded outer basement high (OBH) and a landward dipping, crustal reflector that they interpreted as a splay fault. These authors suggested that the splay fault accommodated the 1958 coseismic slip, and a subsequent seafloor uplift of the OBH was the main source of the associated tsunami. However, only short segments of the SF were clearly identified on the time section, and subsequently the fault geometry and nature of the rocks traversed by the fault were poorly defined. To improve the seismic image, prestack depth migration image (Figure 3a) and velocity model (Figure 3b) of line SIS-44 were constructed by combining information derived from MCS and WA data [*Agudelo et al.*, 2004; *Agudelo*, 2005] (Appendix A).

4. Data Description

[6] The seismic image and velocity model (Figure 3) of line SIS-44 allow interpreting important new geological features, and variations in rock physical properties across the trench and margin. The seismic section we present here has a simple morphology, which, following *Wang and Hu* [2006], can be divided into an outer wedge between km 0 and 25 along the line, with steep surface slope and thrust faults, and an inner wedge east of km 25, where an horizontal, shallow fore-arc basin overlays margin basement rocks.

4.1. Nazca Plate Oceanic Crust

[7] 1. The mafic crust of the oceanic Nazca plate is ∼6.2 km thick (Table 1) and dips 4° landward beneath the trench, 9° down to a 12-km depth beneath the margin, and then 11° down to 20 km. A strong reflector located at a depth of ∼10 km at the western end of the MCS line is tentatively interpreted as the Moho on the basis of WA data
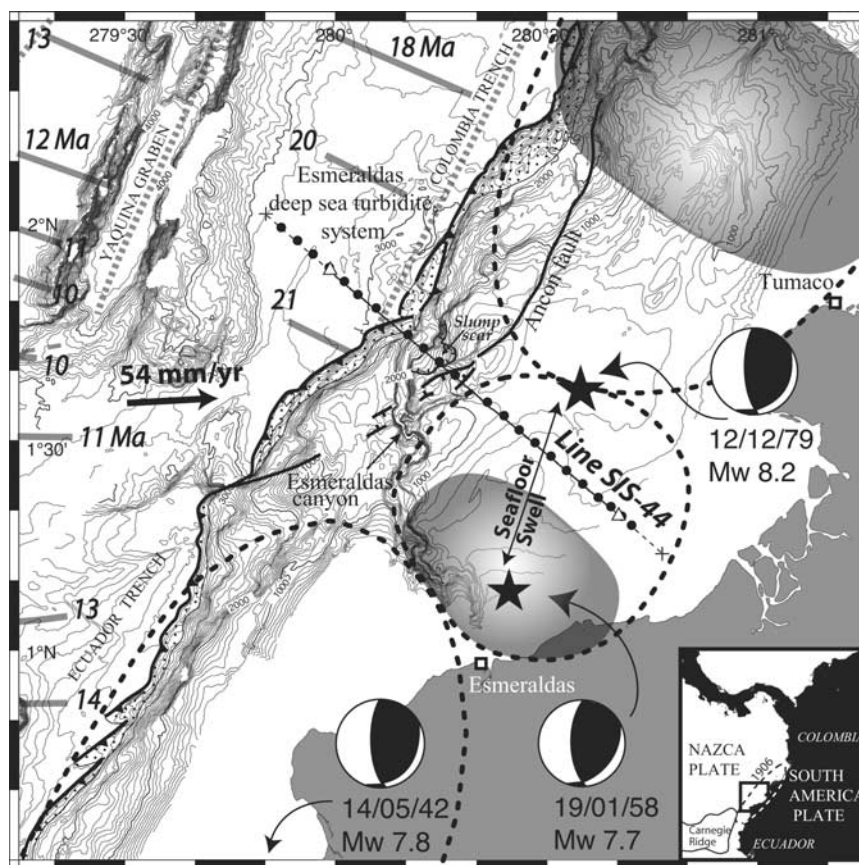
Figure 1. Swath bathymetry of the north Ecuador–south Colombia margin based the Amadeus cruise [*Collot et al.*, 2005], with location of the combined wide-angle (WA) and multichannel seismic reflection (MCS) line SIS-44. Black circles indicate the position of ocean bottom seismometers (OBS) and ocean bottom hydrophones (OBH). Crosses indicate the first and last shots for the WA acquisition profile. White triangles show the position of first and last shots of the coincident MCS profile. Location of the 1942, 1958, and 1979 subduction earthquakes epicenters (stars), rupture zones (dashed ellipses), seismological asperities (gray shaded ellipses), and focal mechanisms (beach balls) are also shown [*Kanamori and McNally*, 1982; *Swenson and Beck*, 1996; *Beck and Ruff*, 1984]. Barbed line is the deformation front, dotted area is frontal wedge, and black arrow is Nazca–South America relative plate motion after *Trenkamp et al.* [2002]. Dashed gray lines are fracture zones, and gray lines with bold italic numbers are magnetic anomalies with ages in Ma after *Lonsdale* [2005] and *Hardy* [1991]. Insert is the location of the study area in South America with the estimated rupture zone of the 1906 earthquake [*Kelleher*, 1972] (dashed ellipse).

(Figure 3a) [*Agudelo*, 2005]. The mafic oceanic crust, which overlies a 7.8 km/s velocity mantle, consists of two high-velocity layers, ocean crust layer A (OCA) and ocean crust layer B (OCB) (Figure 3c and Table 1), with respective average velocities of 5.7 and 6.67 km/s [*Agudelo*, 2005].

4.2. A Rough Oceanic Crust Buried Beneath a Thick Trench Fill

[8] In the trench, a series of high-amplitude and well-bedded reflectors as thick as 3 km is thought to be a turbidite trench fill. The fill is associated with a low-velocity (2.19 km/s) layer designated as SD on Table 1 and Figure 3c. Near the western end of the line, layer SD overlies conformably a powerful reflector (Figures 3 and 4) inferred to be the top of the oceanic crust OCA on the basis of their strong velocity contrast (Table 1). Beneath the trench axis, the oceanic crust is downthrown by large normal faults with ∼1-km-high throws, bounding a 10-km-wide graben

structure. Rocky sequence gs, which fills the graben, ranges in thickness from 1 to ∼1.5 km and is offset vertically by the normal faults. Some of these faults may be reactivated by plate bending as indicated by small vertical offsets that affect the overlaying sequences. Three sedimentary sequences (upper, middle and lower sequences or us, ms and ls on Figure 4) filled the trench and overlay sequence gs. Sequences us and ms, which are 200 to 500 m thick, are weakly deformed and overlie unconformities. Sequence ls reaches a maximum thickness of 2.3 km and shows tectonic deformations. Top laps at its summit unconformity reveal an erosional surface. In contrast with downgoing plate sediment that typically dip landward with the down-flexed surface of the oceanic crust, the dip of sequence ls reverses from landward dipping beneath the trench to seaward dipping beneath the deformation front (Figure 4). Strong reflections and residual diffractions produced by an under-
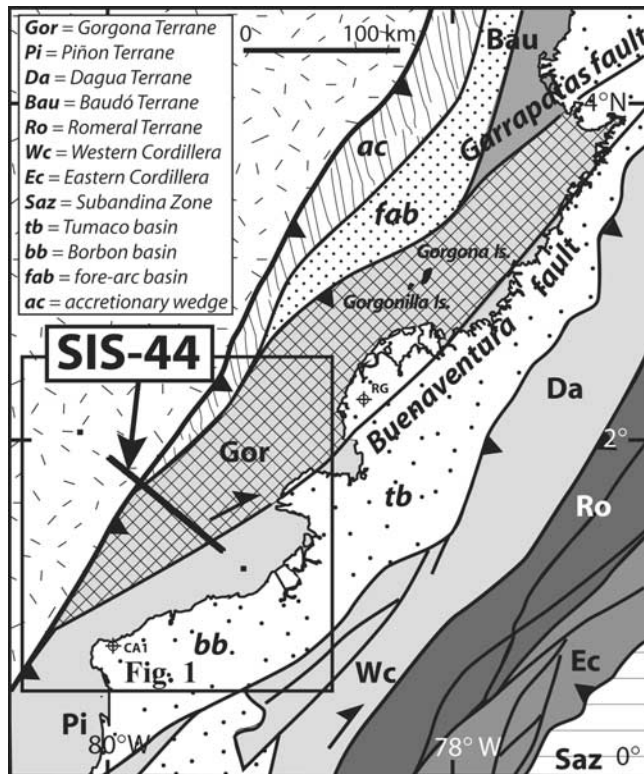
Figure 2. Geological sketch of north Ecuador–south Colombia showing the main accreted terranes, sedimentary basins, and faults after *Cediel et al.* [2003], *Reynaud et al.* [1999], and *Jaillard et al.* [1997]. Note that line SIS-44 cuts across the Gorgona oceanic terrane, which outcrops on Gorgona/Gorgonilla islands [*Dietrich et al.*, 1981; *Kerr*, 2005]. Oceanic basement is known from drill sites Remolino Grande (RG) and Camarones 1 (CA1) [*Marcaillou and Collot*, 2008].

lying complex piece of oceanic crust, with velocities of 3.5–3.8 km/s, suggest that the eastern part of sequence ls is underlain by an oceanic edifice, here interpreted as a 2.5-km-high, buried seamount. However, ocean bottom seismometers (OBS) are too sparse (Figure 1) to confidently model the seamount internal velocity structure. On the basis of MCS lines adjacent to line SIS-44, the seamount and graben are inferred to belong to a trench-subparallel striking, basement ridge-graben structure.

4.3. A Reflectivity-Segmented Interplate Fault

[9] The subduction channel (SC) is used as a generic term [*Shreve and Cloos*, 1986] to designate the interplate low-velocity layer that is squeezed and separated from the overriding and underriding plates by strong reflectors or seismic discontinuities. On the basis of the structural position of the interplate fault in the SC, part of the SC can be interpreted either as a subducting mélange, or underplated sedimentary material. Downdip, the interplate fault and SC show three segments with different seismic characters.

[10] 1. The shallow segment extends from the toe of the margin to a ~6-km depth (km 0–13 in Figure 4). A strong reflector does not underline it, but rather, the stratified trench fill is abruptly truncated eastward by a poorly

reflective fault, interpreted as the décollement thrust De (Figure 4). The décollement dips ~14° landward for ~15 km. It is slightly undulated in its segment associated with the buried seamount, and it forms the roof of a 0.5- to 1.8-km-thick subduction channel that is floored by the reflective top of the oceanic crust. Gentle folding and thrusting deform sequence ls beneath the deformation front but do not affect overlying ms and us sequences. In contrast with poorly reflective fault De, a strong, high-frequency reflector (f1 in Figure 4) splays away from De, at a ~25° angle, before to shallowing to 12° and reaching the seafloor above the décollement. This reflector shows a reverse seismic polarity and is interpreted as an active thrust fault that separates overlying reflective and landward tilted sediment from underlying less reflective and deformed accreted material.

[11] 2. The intermediate segment of the plate interface extends between 6- and 9-km depths (km 13–26 in Figure 3). Unfortunately, the roof and floor of the SC are poorly reflective on MCS data, so that its shape could not be resolved. The shadow zone observed in the OBS record sections between waves refracted in the margin basement (Pg) and those refracted in the lower plate (Pc) [*Gailler et al.*, 2007] is interpreted as a low-velocity zone in the vicinity of the plate boundary [*Agudelo*, 2005]. However, the parameters of the low-velocity zone are nonunique. Because the SC can be interpreted from MCS data along the upper and deep segments of plate interface, we have considered that the SC does exist along the intermediate plate interface segment, although it does not return clear vertical reflections on MCS data. Wide-angle phases reflected from the base of the low-velocity zone and from the oceanic Moho (PmP) were observed [*Gailler et al.*, 2007] and modeled using travel time with velocities ranging from 3.7 to 4 km/s to fit the data [*Agudelo*, 2005]. On the basis of wide-angle reflections on top of the oceanic crust, the floor of the SC is estimated to dip ~9° landward (Figure 3b).

[12] 3. The deep segment of the plate interface returns strong, but discontinuous reflections, which together with wide-angle reflections and refracted arrivals from the underlying oceanic crust were used to constrain the geometry and velocity of the SC. From ~9- to 15-km depths (km 26–56, Figure 3a), the velocity of the SC varies from ~3.5 to 4.0 km/s, thus forming a low-velocity zone relative to overlying 4.5–5.5 km/s basement rocks (Table 1). The thickness of the SC varies irregularly between 0.6 and 1.3 km, before decreasing to less than the MCS seismic vertical resolution (~90 m) near a 15-km depth. These characteristics are similar to those observed along the Japan margin [*Tsuru et al.*, 2002]. The roof of the SC dips at an ~11° angle, whereas the dip of its base increases from 9° to ~11° at a depth of 11–12 km (Figures 3b and 5). Near a depth of 11–15 km, the SC shows internal, sigmoid reflectors that form toplaps beneath a continuous landward dipping surface. Despite possible diffractions, these reflectors are well constrained as indicated by IsoX panels (Appendix B). The reflectors tend to dip locally opposite to the plate interface (Figure 5), and are compatible with imbricated layers that were likely truncated by a roof thrust. Deeper than 15 km, the strongest reflectors are interpreted as the top of the oceanic crust, and the migrated image suggests a near constant SC dip of ~11°.
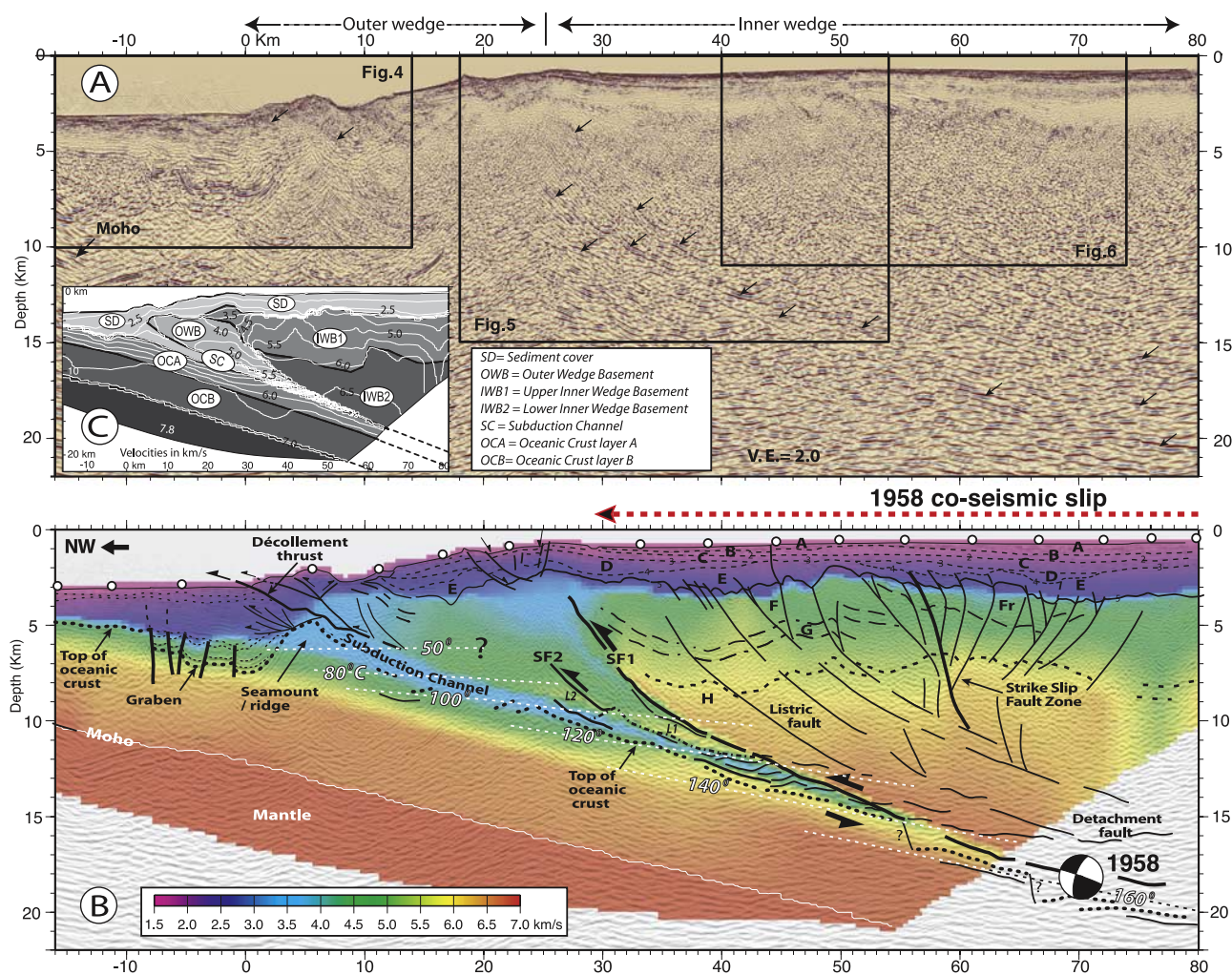
Figure 3. (a) Color-coded, prestack depth-migrated MCS line SIS-44 across north Ecuador–south Colombia margin. Seismic section is displayed with automatic amplitude gain. Frames indicate zooms. (b) Final blocky velocity-depth model and line drawing overlain over PSDM image to highlight relationships between velocity and structural features. Open circles along seafloor are ocean bottom seismometers. SF1 and SF2 are splay faults. Fore-arc basin includes sedimentary layers A to E [after *Marcaillou and Collot*, 2008], and margin basement encompasses layers F to H. Numbers along thin black dashed lines are major stratigraphic unconformities. Fr is inverted graben. Note the low velocity in the SC and the strong lateral velocity contrast across SF1. The 1958 focal mechanism [*Swenson and Beck*, 1996] is projected on the interplate fault. Seaward extent of 1958 brittle coseismic slip matches with splay fault SF1. White dash lines are isotherms in °C projected from thermal model calculated for adjacent line SIS-42 [*Marcaillou et al.*, 2006]. (c) Blocky velocity model from *Agudelo* [2005] showing velocity layers and isovelocity contours in km/s. Physical parameters of each layer are shown in Table 1.

4.4. A Splay Fault Zone and Associated Listric Normal and Reverse Faults

[13] Migrated image (Figure 5) reveals two strong reflections SF1 and SF2 that dip landward at 33° and 26° between km 24 and 34, before soling out at 12- and 10-km depths on the roof of the SC, respectively, with 15 and 17° angles. SF1 is remarkably associated with a major and sharp basement lateral velocity discontinuity that juxtaposes high-velocity (5–6.6 km/s) rocks of the inner wedge basement, with 4–4.5 km/s rocks of the outer wedge (Figure 3b) [*Gailler et al.*, 2007; *Agudelo*, 2005]. SF1 appears to be the reflective trace of the splay fault interpreted by *Collot et al.* [2004]. As interpreted by Collot et al., the splay fault is associated with

a gentle rise of the seafloor and a summit graben, which is aligned with the Ancon Fault (Figure 1), and deforms fore-arc basin sediment across the trench slope break. The graben is controlled by asymmetric normal faults that extend down to ~2 km below seafloor, and offset vertically the basement by as much as 600 m (Figure 5). Seafloor scarps, 100- to 200-m-high, associated with the faults may reveal Quaternary reactivations. West of the graben, the seaward tilted segment of the fore-arc basin shows an amphitheater-shaped indentation (Figure 1) indicating massive submarine landslides [*Ratzov et al.*, 2007].

[14] Landward of SF1, the high-velocity basement is tentatively characterized on the basis of its internal reflec-

Table 1. Velocity Parameters and Average Thickness for Each Layer of the North Ecuador–South Colombia Margin and Subducting Oceanic Crust[a]

| Unit | Average Velocity (km/s) | | | | |
	Top of Layer	Bottom of Layer	All of Layer	Average Gradient (1/s)	Thickness (km)
Sedimentary cover (SD)	1.79	2.59	2.19	0.34	2.03
Upper inner wedge (I WB1)	4.29	5.45	4.87	0.25	5.08
Lower inner wedge (I WB2)	5.72	6.46	6.09	0.14	7.02
Outer wedge (OWB)	3.72	5.00	4.36	0.29	4.44
Subduction channel (SC)	3.81	3.77	3.79	−0.04	0.93
Ocean crust A	4.92	6.49	5.7	0.72	2.2
Ocean crust B	6.5	6.85	6.67	0.09	4

[a]See Figure 3c [after *Agudelo*, 2005]. Because of high lateral variability in velocity and thickness, parameters for OWB layer are taken at x = 25 km along the transect (Figure 3c). Because of ray coverage and geometry, average velocity and thickness for IWB1 and IWB2 units are taken between x = 50 and 60 km.

tivity and structural patterns (Figure 5). Highly reflective rocks in the form of the ~600-m-thick band G and the deep foundation H of the margin, contrast with rocks F of lower reflectivity. Band G and the roof of rock foundation H appear to have been concomitantly and conformably deformed by large, landward dipping faults outlined by discontinuous reflectors. The large westernmost intrabasement fault, which parallels SF1, can be interpreted as a listric normal fault on

the basis of its curved geometry and normal throw across both H and G at km 36–40 (Figure 5). Between km 39 and 49, other faults with similar dips to SF1 can be interpreted as reverse faults on the basis of their vertical offset relative to dip direction, and folding pattern of band G and roof of rocks H (Figure 6). The faults offset locally the basement top F that is outlined by major unconformity U5, and root at a 16-km depth on a strong subhorizontal reflector (Figure 3b). Overall the basement faults landward of SF1 are considered inactive, as they do not deform the fore-arc basin strata, thus supporting a presubduction, strongly structured basement. Outer wedge rocks located between SF1 and SF2 exhibit a series of relatively strong, landward dipping reflections, whereas the rocks between km 14 and 24 are poorly reflective (Figure 3). However, between km 22 and 42, immediately above the SC, the foundation of the outer wedge consists of landward dipping, 0.8- to 1.5-km-thick rock lenses (L1–L2 in Figure 3b) characterized by high 5–5.5 km/s velocities (Table 1) and strong reflectors.

4.5. A Fossil Strike-Slip Fault Zone

[15] The seismic line cuts across a broad seafloor swell only 250 m high, which correlates at depth with a wide basement rise, and split the fore-arc basin in two depocenters. According to the interpretation by *Marcaillou and Collot* [2008] the fore-arc basin contains five sedimentary units (A to E) separated by seismic unconformities U1–U4. The units are characterized by velocities ranging from 1.6 to 2.9 km/s and rest over a 4.29 km/s basement unit F [*Agudelo*, 2005] from which, unit E is separated by unconformity U5 (Figure 6). Sediment reaches ~2.5 and 3 km in thickness beneath the western and eastern
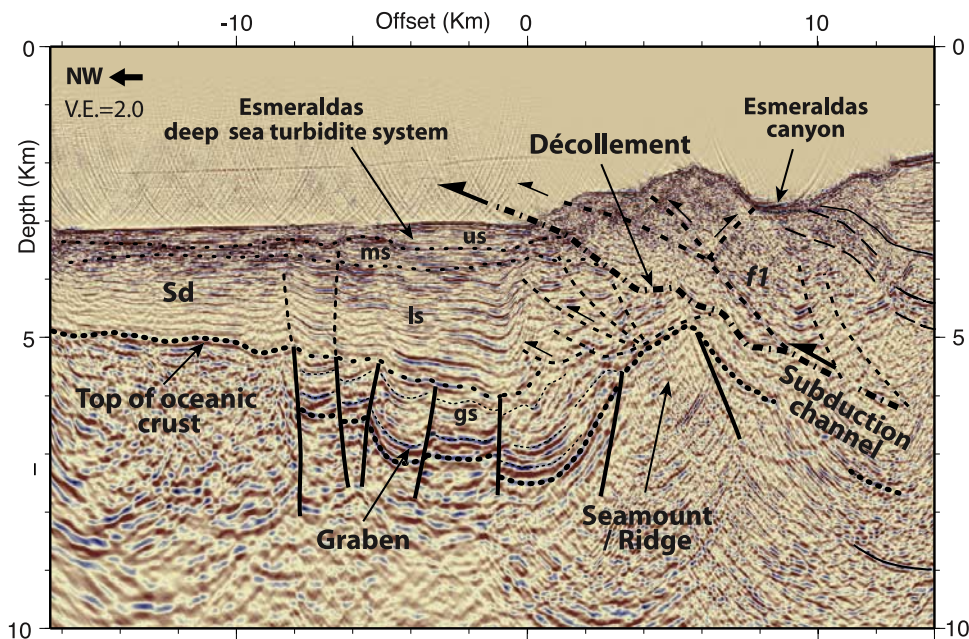
Figure 4. Close-up of PSDM line SIS-44 showing crustal structures beneath the Colombia trench and deformation front. Location is shown in Figure 3. A 3-km-thick trench fill (sequences ls, ms, us) overlies a 1.5-km-thick (sequence gs), filled tectonic graben. Subduction of a buried seamount forces the décollement thrust to rise, preventing the development of an accretionary wedge; f1 is a major reflective thrust fault. Note the most recent, 0.4-km-thick us sequence of the Esmeraldas deep-sea turbidite system, and incipient folding and thrusting in the wake of the subducting seamount.
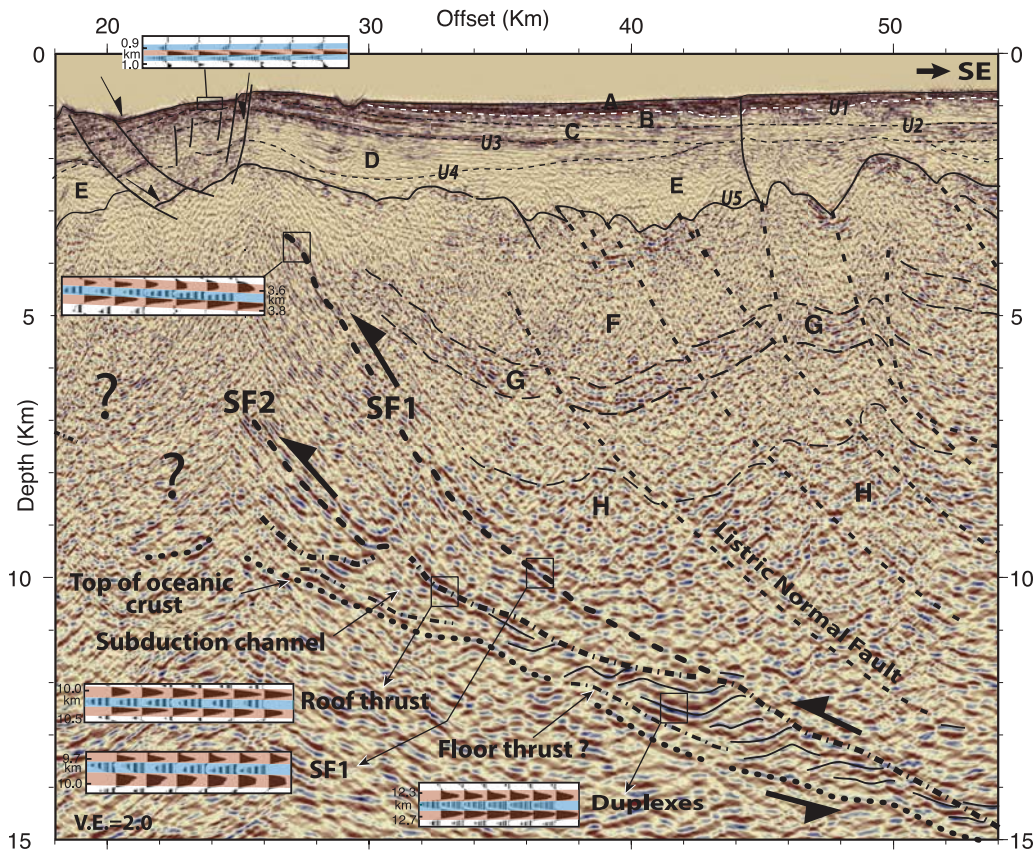
Figure 5. Close-up of PSDM line SIS-44 across the splay faults and subduction channel. Location is shown in Figure 3. Layers A to H as in Figure 3. U1–U5 are stratigraphic unconformities. U5 is top of oceanic basement. SF1 and SF2 are interpreted splay faults. Note ~0.3-km-thick internal subduction channel structures with subhorizontal or seaward dips interpreted as duplexes. Vertical offsets across band G and rocks H suggest ancient listric normal faults. Similar faults may have been inverted in the east part of the close-up (km 40–50). Insets show negative polarity (red-blue-red) of the strongest splay fault SF1 and plate boundary reflections (roof thrust and duplexes) compared to positive polarity (blue-red-blue) of the seafloor. Negative polarity reflections strongly suggest fluids in the fault zones.

depot centers, respectively (Figure 3). Between km 54 and 64, deepest unit E reveals remarkable, well stratified and strongly reflective patches of sediment, which show sharp lateral and steeply inclined terminations, suggesting that strata are truncated by a fault with a thrust component, and juxtaposed against beds of lesser reflectivity (Figure 6). The top of underlying basement F is similarly offset vertically by reverse separation faults. The faults, which have juxtaposed blocks of different thicknesses (Fr in Figure 6), extend downward in the basement, where they show a switch in dip from steeply landward to seaward dipping. These faults appear to merge at depth, together with adjacent faults to the west that dip steeply landward. The resulting overall fault pattern produces a positive flower structure or contractional duplex [*Woodcock and Fisher*, 1986; *Harding*, 1990] typical of a strike-slip fault zone that has juxtaposed rocks of different reflectivity or with abrupt variations in thickness [*Allen and Allen*, 1993]. Between km 64 and 74, other basement faults, which dip strongly seaward with a normal throw, could be part of the flower structure. Down deep, the flower structure roots at a ~10-km depth, on a large, landward dipping, listric normal fault. It is interesting to note that the flower structure is associated with a reflective

and roughly stratified body Fr (Figure 6) that has locally formed over unit F between km 52 and 72. This body is thickest (~2.2 km) along its median axis at km 60–66, and structurally segmented by steeply dipping faults. Accordingly, this body is interpreted as a former graben or rift zone once controlled by high-angle normal faults.

5. Discussion

5.1. Seamount/Ridge Subduction: A Factor for Subduction Erosion and Earthquake Nucleation

[16] The basement ridge-graben structure identified on line SIS-44 can be interpreted as a remnant NNE trending fracture zone, similar to the Yaquina graben (Figure 1). The structure could be part of the spreading transform system that created the Neogene Nazca plate oceanic crust [*Lonsdale*, 2005; *Hardy*, 1991], according to the model proposed by *Sallares and Charvis* [2003].

[17] Ridge or seamount subduction has been shown to leave large scars in the inner trench slope in the form of subcircular indentation [*Collot and Fisher*, 1989; *Masson et al.*, 1990] or furrows that are collinear with plate convergence [*von Huene et al.*, 2000]. Line SIS-44 shows that the
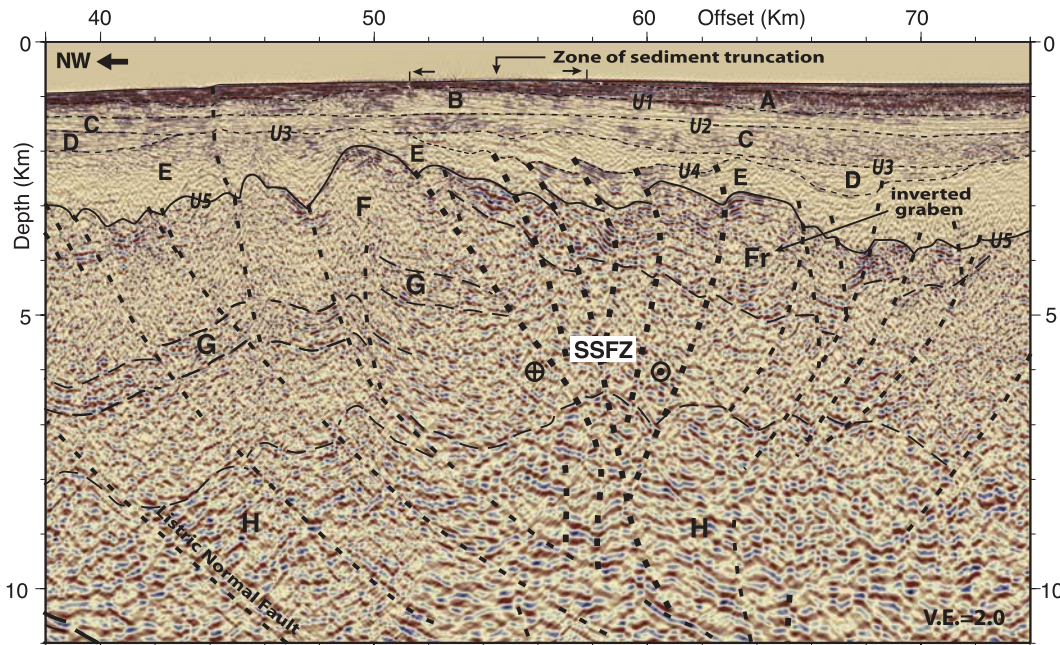
Figure 6. Close-up of PSDM line SIS-44 across an ancient transpressive, strike-slip fault zone (SSFZ). Location is shown in Figure 3. Heavy dashed lines are steeply dipping reverse separation faults associated with a positive flower structure, a broad basement rise, and seafloor swell. Layers A to H are as in Figure 3. Fr is inverted graben. Sediment truncation at the seafloor swell reflects broad uplift possibly associated with underplating or deep-seated contraction strain.

subduction of a 2.5-km-high seamount has not produced a large slope indentation, because the thick trench fill obliterates the seamount relief (Figure 4).

[18] Seamounts are considered as major agents enhancing rates of subduction erosion [*Scholl et al.*, 1980] as they are capable of fracturing margin rocks [*von Huene and Lallemand*, 1990; *Fisher et al.*, 1991; *Collot et al.*, 1992; *Dominguez et al.*, 2000] and thin, possibly by hydrofracturing processes, the underside of the margin [*von Huene et al.*, 2004; *Ranero and von Huene*, 2000]. Using 3-D migrated seismic data across Nankai accretionary wedge, *Bangs et al.* [2006] interpreted the detailed process of subduction erosion preceding sediment underplating as a result of a basement ridge subduction. On line SIS-44, an indirect observation supports basal tectonic erosion. Seaward of the trench slope break, the seafloor and stratification of the fore-arc basin dip sharply trenchward 5° (Figure 7b) and are affected by shallow landslides (Figure 1) [*Collot et al.*, 2005; *Ratzov et al.*, 2007], arguing for a postsedimentation, trenchward tilt. Back tilting the rotated segment of the fore-arc basin (Figure 7a) indicates that by the end of unit C deposition, the margin extended at least 10 km farther seaward than to today. This interpretation implies thinning of the outer margin wedge by basal tectonic erosion.

[19] The subduction of the buried seamount has significant implications on the structural evolution and dynamics of the margin. The décollement and associated faults are forced to rise upward at a relatively high angle above the seamount, impeding tectonic accretion (Figure 4). Sandbox modeling [*Dominguez et al.*, 2000] predicts a shadow zone in the wake of a subducting seamount so that the trench fill is conveyed into the subduction channel in the tectonic

wake of the seamount, rather than being frontally accreted. Such a mechanism likely accounts for the absence of an accretionary wedge between latitudes 1°30'N and 2°0'N, despite the thick trench fill (Figure 1). However, the gentle deformation affecting the trench fill in the wake of the seamount together with the truncation of the trench fill by the décollement, and the overlying thrust sheet, advocate incipient tectonic accretion. The subducting seamount controls the size of the inlet to the SC, so that the sediment input thins dramatically from a 4.5-km-thick trench fill including the graben fill, to <0.5 km above the seamount (Figure 4). This strong and abrupt change in sediment supply implies tectonic adjustment of the SC and overriding plate, as well as a highly variable volume of pore water dragged in the subduction zone. As proposed by *Sage et al.* [2006] in central Ecuador, a nonsteady rate of sediment supply to the SC is likely to introduce frictional heterogeneities along the plate interface and have an effect on earthquake initiation and rupture propagation.

[20] According to *Cloos* [1992], subducting seamounts may generate large subduction earthquakes. Because of their shape and buoyancy, large seamounts are believed to modify shear stress along the interplate contact [*Scholz and Small*, 1997]. They could be decapitated in the seismogenic zone, thus producing a large earthquake, and correlating with the seismological asperities, such as defined by *Lay et al.* [1982]. Such a seamount has been imaged by tomography at a 30-km depth within the rupture zone of Costa Rica [*Husen et al.*, 2002]. Because it is deeply buried and hence protected by trench fill sediment and the frontal wedge, the seamount on line SIS-44 does not show, at a seismic scale, internal deformation resulting from underthrusting. Rather,
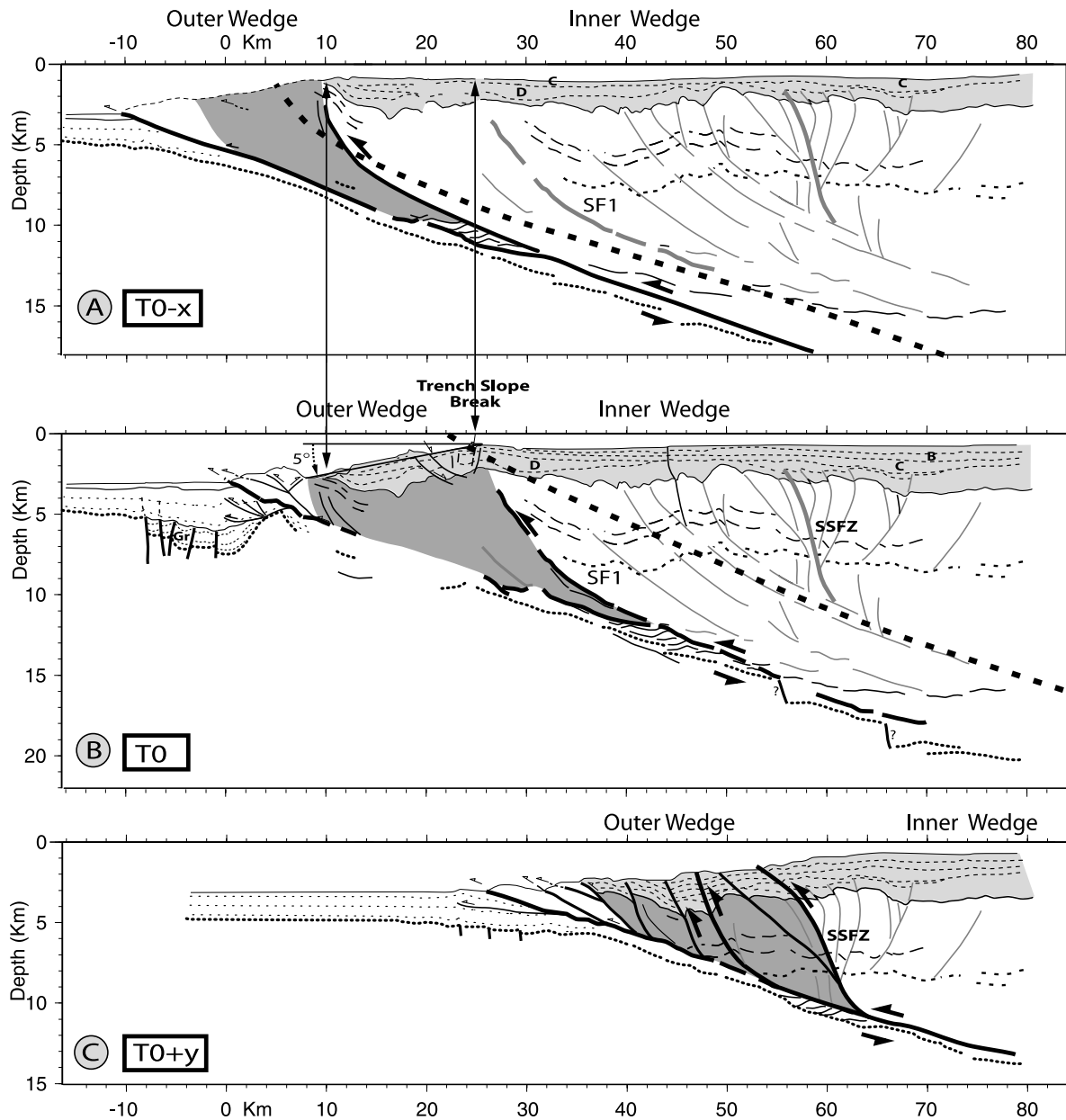
Figure 7. Diagram showing likely structural evolution of the studied segment of the north Ecuador–south Colombia margin, through basal erosion, underplating, and reactivation of ancient listric normal and strike-slip faults as a mechanism for controlling subduction earthquake ruptures. Bold black lines and gray lines are active and inactive faults, respectively. Grey shaded areas are outer wedge basement rocks expected to be locally altered by deep-sourced fluids flowing along crustal faults. (a) Inferred margin structures at time of unit C deposition (T0−x). The westernmost part of the fore-arc basin has been back rotated to its initial subhorizontal position. SF1 is a listric normal fault not yet in contact with plate interface. Rocks beneath heavy dashed line are bound to be destroyed by subduction erosion between times T0−x and T0. (b) Present-day margin structures (at T0) from line SIS-44. Rocks beneath dashed line are to be destroyed by subduction erosion between times T0 and T0+y. Subduction erosion will result in destruction of present-day active structures, reactivation of ancient faults and margin subsidence. (c) Ancient listric normal fault and the strike-slip fault zones (SSFZ) are reactivated under compressive stress at Time T0+y as they become tilted trenchward and put in contact with plate boundary fault.

deformation appears to be accommodated by the frontal wedge and the SC, which is interpreted to be ~1.3 km thick, ahead of the seamount (Figure 3b). These observations suggest that during its impending tectonic burial, the seamount will establish new stress conditions between km 9 and 24 along line SIS-44, so that the seismogenic zone, which is discussed in the next part, will extend farther updip than today. As shown by *Bangs et al.* [2006], a subducting seamount can preserve a coherent shape as deep as 8 km below seafloor, so that the seamount in line SIS-44 could alternatively reach the present-day seismogenic zone prior to potential shearing off and underplating. This later interpretation is in agreement with the proposal by *Cloos and Shreve* [1996] that a seamount could trigger a large earthquake providing that it be transported to the seismogenic zone protected by a shield of sediment. We speculate that other features of similar or greater size to that identified in line SIS-44, embedded in subducting sediment may have been transported deeper into the seismogenic zone, where they could be responsible for the 1958 earthquake seismological asperity (Figure 1).

5.2. Nature of the Interplate Fault

[21] We interpret the poorly reflective upper and intermediate segments of the interplate fault, and its more reflective, deeper segment, as the aseismic updip segment, and the seismogenic zone of the interplate fault, associated with the outer and inner wedges [*Wang and Hu*, 2006], respectively. The updip fault segment is generally inferred to be mechanically weak, aseismic [*Byrne et al.*, 1988], and unaffected by coseismic slip during great earthquakes, depending on its thermal regime and fault dip [*Hyndman et al.*, 1995]. In contrast with the commonly highly reflective décollement thrusts and top of oceanic crust beneath large accretionary wedges [*Bangs et al.*, 2004; *Shipley et al.*, 1994], the updip segment of the north Ecuador plate boundary fault between 6- and 9-km depths is difficult to recognize because of poor reflection amplitudes. Such a low reflectivity was also observed off SW Japan (Nankai margin) along the décollement thrust at a depth of 6−7 and 9−10 km. The low amplitude may be due to interference arising from a seafloor multiple [*Park et al.*, 2000], or poorly reflective zones associated with the interpreted formation of duplex structures [*Park et al.*, 2002b]. Considering seismic amplitudes in sediment as indicative of sharp contrasts in porosity and fluid content, the poor reflectivity of the décollement along line SIS-44 may indicate that the updip segment of the SC is depleted in fluids, and consequently lacks substantial excess pore pressure. However, seismic artifacts and scattered energy produced by structural complexities of the downgoing plate are likely responsible for the poor seismic amplitudes, and preclude any direct conclusion. The SC velocity of ~3.5−3.8 km/s partially overlaps velocities of the oceanic crust, possibly indicating that lower oceanic plate or outer wedge rock fragments were incorporated into the SC mélange. Whatever the lithology of the SC may be, its 3.5−3.8 km/s velocity with mean porosities no higher than 10−15% according to the velocity-porosity analysis conducted in the SC of southern Ecuador by *Calahorrano et al.* [2008] supports a low fluid content in the updip segment of the SC. When entering the SC, sediment shows 1.8−2.6 km/s velocities (Table 1), compatible with a 30−40%

average porosity with respect to results published by *Calahorrano et al.* [2008]. The porosity drop between trench sediment at 4−5 km depth and the SC at 6−8 km depth suggests that fluids were either expelled seaward due to sediment compaction and good drainage along the SC, or they invaded fractures and acted to disintegrate the fabric of the overlaying basement [*Behrmann*, 1991; *Le Pichon et al.*, 1993; *von Huene et al.*, 2004; *Ranero et al.*, 2008]. In absence of substantial excess pore pressure, the effective pressure and fault shear stress should be relatively higher [*Le Pichon et al.*, 1993]. However, the limited seaward extent of the 1958 seismic rupture zone (Figures 1 and 3b) implies that the updip segment of the interplate fault did not rupture elastically during the event, and is therefore considered weak and aseismic. This weak segment will briefly become stronger during a great earthquake [*Wang and Hu*, 2006].

[22] The downdip transition from a poorly reflective to reflective SC around a 9- to 10-km depth and ~100−120°C, is interpreted to reflect the onset of a range of processes associated to the aseismic-seismic transition. These processes include shear localization, increased consolidation state of fault gouge, fluid release from diagenetic transformations and low T metamorphism of subducting sediment as proposed by *Saffer and Marone* [2003], *Hyndman et al.* [1997], and *Moore and Saffer* [2001], as well as a change in tectonic process from basal erosion to duplex formation, and underplating [*Bangs et al.*, 2004]. As inferred from seismic inversion of the 1958 earthquake [*Beck and Ruff*, 1984] the updip limit of the seismogenic zone extends somewhere beneath the outer inner wedge or trench slope break (Figure 3b), where the wedge taper, which is the angle between the surface slope and the dip of the interplate fault, changes from 16 to 17° beneath the outer wedge to ~11° beneath the inner wedge. Similar observations were made for the Nankai accretionary wedge, where the updip limit of the seismogenic zone is associated to a change in wedge taper and a step down of the décollement thrust [*Kimura et al.*, 2007]. Accordingly, along line SIS-44, the updip limit of the seismogenic zone could include both the deeper part of the reflective segment of the SC and the associated root zone of the splay fault.

[23] The inner wedge is generally considered stable [*Wang and Hu*, 2006], as fore-arc basin sedimentation helps stabilizing the wedge by preventing internal basement deformation [*Fuller et al.*, 2006]. On line SIS-44, the broad, 250-m-high seafloor swell (Figure 1) centered on the fore-arc basin reveals however, sediment truncations at the seafloor suggesting a broad and recent uplift (Figure 6). This broad uplift could result from sediment underplating or cumulative, and permanent deep-seated contraction deformation, associated with repeated interplate earthquakes (Figure 1) thus supporting some degree of inner wedge anelastic deformation, possibly associated with reactivation of the SSFZ (Figure 6).

5.3. Nature of the Splay Fault

[24] *Collot et al.* [2004] suggested that the brittle coseismic slip likely propagated along SF1, because intramargin faults as SF1 could accumulate and release considerable tectonic stress, in contrast with thrusts in semiconsolidated sediment [*Cummins et al.*, 2001]. On the basis of investigations of the Shimanto belt in Japan, brittle coseismic slip

is believed to have produced cataclasis and friction melting, i.e., pseudotachylytes [*Ikesawa et al.*, 2003] along a discrete fault interpreted as the roof thrust of the Mugi Mélange [*Kitamura et al.*, 2005]. This process occurred at 6- to 8-km depths, under maximum temperatures of 180–200°C as determined from vitrinite reflectance [*Kitamura et al.*, 2005]. *Mukoyoshi et al.* [2006] also reported formation of pseudotachylyte at depths of 2.5–5.5 km, and 160–240°C along an out-of-sequence thrust system in the Shimanto belt, thus supporting brittle failure along splay faults in an accretionary complex. In northern Ecuador, the temperature and depth burials of splay fault SF1 and deep segment of the SC appear lower than the temperature and greater than the depth burials of the splay fault in the Shimanto accretionary complex. According to thermal modeling [*Marcaillou et al.*, 2006], splay fault SF1 cuts the thermal structure between ~50°C and 140°C at depths of 6–15 km, and the failure of the 1958 earthquake initiated at 160–170°C, and ~19-km depth, where the plate interface tends to parallel the thermal structure (Figure 3b). Such differing depths and temperatures along splay faults in Japan and Ecuador may be explained by the diverse methods used to determine fossil and present-day temperatures, but also by their different fault dip geometry, lower plate age, and contrasting basement rheologies and mineralogies, i.e., sedimentary in Japan and oceanic in Ecuador. However, consistently with observations in the Shimanto belt, seismic slip could have produced pseudotachylyte along the Ecuador interplate fault deeper than 15 km, and possibly along a splay fault (SF1) in an oceanic basement.

[25] Active splay faults locally propagate to the seafloor as shown west of Kii Peninsula in Japan [*Moore et al.*, 2007]. In line SIS-44, neither SF1 nor SF2 reaches the seafloor, which suggests that if we assume the hypothesis that the 1958 coseismic slip was diverted up the splay fault, the slip strongly decayed upward along the splay fault. This decay may be due either to the distribution of the slip across both SF1 and SF2 faults, or to the strongly curved geometry of SF1. The 33° dip of the uppermost segment of SF1 provides a larger normal stress than that across the 15° dip lowermost fault segment, facilitating the upward decay of the slip. Modeling the tsunamogenic seafloor displacement in the western Nankai Trough, as the result of slip on a splay fault, *Cummins and Kaneda* [2000] showed that rupture need not have a seafloor geologic expression to generate a large tsunami, and could terminate at a 3-km depth below seafloor. Therefore, it is possible that the 1958 earthquake thrust rupture, which triggered a tsunami [*Espinoza*, 1992], uplifted the seafloor at the trench slope break, and reactivated indirectly normal faults of the summit graben so that examination of their surface rupture could help understanding of earthquake processes as suggested by *Henstock et al.* [2006] for the toe of the Sumatra margin.

5.4. Sediment Underplating: A Process Possibly Controlled by Overlapping Segments of the Interplate Fault

[26] The internal structure of the SC in the updip part of the seismogenic zone has been interpreted from seismic data and analysis of onshore analogs [*Sample and Fisher*, 1986], as landward dipping duplexes [*Kitamura et al.*, 2005; *Ikesawa et al.*, 2005]. The duplexes form seaward by incorporating sections of the subducting mélange as the décollement thrust steps down, thus forming a stack of seaward verging, underplated material characterized by small relative displacements (Figure 8a) [*Hashimoto and Kimura*, 1999; *Ikesawa et al.*, 2005; *Kitamura et al.*, 2005; *Kimura et al.*, 2007]. In this model, the youngest duplex form updip, at the leading front of the stack. In the SC of line SIS-44, the low-velocity, imbricated layers that formed between 9- and 15-km depths, are inferred to be forward dipping duplexes with local antiformal stacks according to their seismic image and the example of the Dundonnel structure interpreted by *Boyer and Elliott* [1982] (Figure 8b). Despite the lack of seismic resolution to fully define the duplexes and their floor thrust, we propose a model for forward dipping duplex formation. In this model, most of segment Sc1 of the SC (Figure 8c) is roofed by the active interplate thrust that branches upward on SF1, and floored by the décollement thrust. As in the Dundonnel structure [*Boyer and Elliott*, 1982], the youngest horse would form at the back of the stack, where SF1 roots on the interplate fault, thus supporting that Sc1 is a zone of active growth of duplexes that develops dominantly from the subducting mélange. We speculate that splay fault SF1 forces the underlying décollement thrust to step down, leading to underplating and progressive seaward migration of duplexes. In this model, segment Sc2 of the SC comprises the oldest duplexes characterized by large relative displacements. According to our model the duplexes would form between overlapping segments of the interplate fault at a depth of ~14–15 km and under ~120–140°C temperatures.

[27] Stress fluctuations during the earthquake cycle strongly affect the wedge mechanics [*Wang and Hu*, 2006] and, in our hypothesis, may account for the process of duplexes formation. According to *Scholz* [1998] and *Wang and Hu* [2006], the updip interplate fault segment has opposite mechanical behavior to the seismogenic zone during earthquake rupture. The seismogenic zone, which is weak and supposed to be locked during the interseismic period, is velocity weakening, that is, its coseismic stress drop and slip are accompanied by a decrease in the fault frictional resistance. The updip fault segment or décollement thrust apparently has a slip strengthening behavior meaning that its strength will increase when it is forced to slip by rupture of the seismogenic zone, so that this fault segment will tend to oppose slip. *Wang and Hu* [2006] proposed that the updip segment will likely creep during the postseismic period, when the basal shear stress drops, and compressive elastic strain accumulated during the coseismic phase is progressively released seaward thus leading to frontal accretion, permanent deformation and basal erosion. We propose a model assuming that velocity strengthening behavior of the décollement thrust extends to depths of ~15 km and temperatures of 120–140°C (Figure 3b). We consider that at depths of 14–15 km, the subducting mélange consists of less than 10% porosity, based on velocity models [*Calahorrano et al.*, 2008], lithified sedimentary rocks capable of storing some elastic energy. In this model, duplexes would form through a two-step process: (1) brittle coseismic slip along the root zone of the splay fault increases stress along the underlying décollement, and both thrusts, and weakens the subducting mélange by increasing its pore fluid pressure; and (2) during the post-
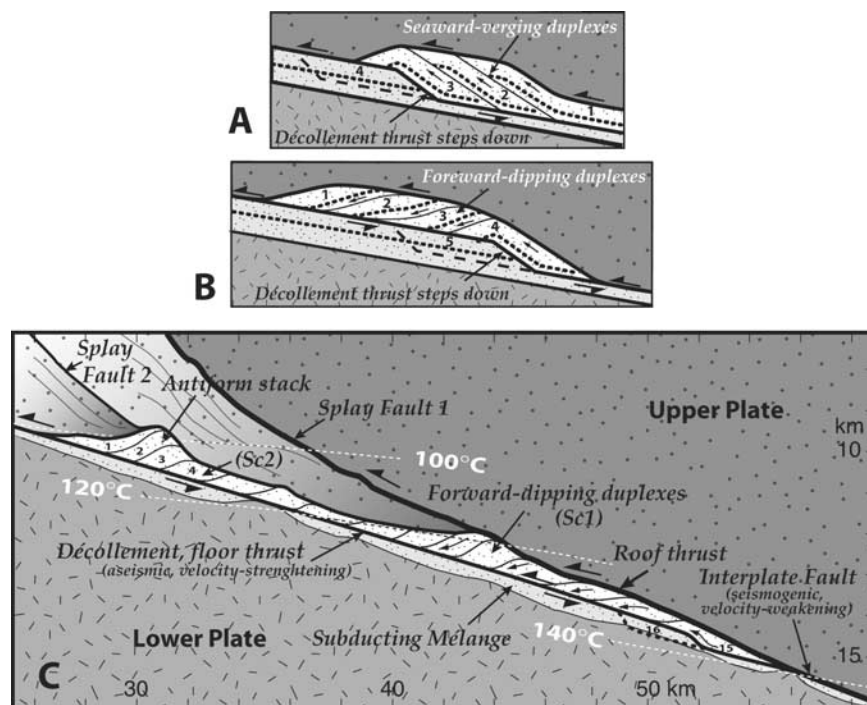
Figure 8. Schematic diagram showing (a) typical development of seaward verging duplexes characterized by relatively small subhorizontal displacement and (b) forward dipping duplexes characterized by relatively large displacement [after *Boyer and Elliott*, 1982]. Note that numbers represent order of development 1, oldest; 4, youngest. (c) Interpretative model of forward dipping duplexes within the low-velocity SC in the updip portion of the seismogenic zone of line SIS-44. Duplexes develop in Sc1 from subducting mélange and oceanic crust between the seismogenic roof thrust (deep section of SF1) and aseismic floor or décollement thrust. Merging SF1 with the interplate fault forces underlying décollement thrust to step down, leading to duplex formation. During formation a horse climbs upward from its basal contact with/within the oceanic crust onto the décollement thrust cutting steeply through the subducting layers. The resulting duplex consists of downward facing horses and antiformal stacks. Horse 1 is oldest visible. Older horses could have been destroyed by subduction erosion. Note that isotherms [*Marcaillou et al.*, 2006] crosscut the splay faults and tend to parallel the interplate fault.

seismic phase, seaward stress relaxation would tend to facilitate deformation of the subducting mélange and the formation of a new horse. Multiple earthquake cycles would be, however, necessary for a horse to detach from the subducting mélange and climb up the décollement thrust to stack beneath the previous horse (Figure 8c).

5.5.   Origins and Implications of Margin Basement Rocks and Structures

[28]   Understanding the origin of intrabasement crustal faults may provide a clue for the cause of the presently active splay faults and requires unraveling the origin and the structural development of the margin basement.

5.5.1.   Margin Basement Rocks and Their Mechanical Strength

[29]   The oceanic plateau origin of the inner wedge margin basement is substantiated by geochemical affinities of oceanic rocks that crop out on Gorgona island [*Storey et al.*, 1991; *Kerr*, 2005], and by the contrast between the high- and low-velocity gradients in the upper (IWB1, Figure 3c) and lower (IWB2, Figure 3c) high-velocity layers of the margin basement (Table 1) [*Agudelo*, 2005]. Such a contrast

is commonly associated with magmatic underplating contributing to the growth of the lower layer of oceanic plateaus [*Caress et al.*, 1995; *Charvis et al.*, 1999]. However, basement rock velocities and seismic structures (Figure 3b) differ greatly across SF1 indicating an abrupt change in rock nature or alteration and shear strength beneath the outer and inner wedges. Physical properties of basement rocks west of SF1 were either acquired during the plateau formation or resulted from later construction or alteration. The outer wedge basement rocks are pre-Eocene because they are overlain by the oldest fore-arc basin seismic unit E inferred to be Eocene or older in age [*Marcaillou and Collot*, 2008]. The 4.36 km/s average velocity of OWB (Table 1) may either reflect ancient sediment or various types of volcanic rocks. With the exception of its toe (km 0– 10 Figure 4), the OWB does not show the classical imbricate structure of an accretionary wedge, and the late Cretaceous to Paleogene history of the Gorgona terrane is likely to have been intraoceanic [*Kerr and Tarney*, 2005], and hence is not compatible with the development of a large accretionary wedge. Although a sedimentary contribution to the lithology of OWB is plausible, an overall oceanic nature

is likely on the basis of its internal velocity (up to 5.0 km/s, Table 1) and large variety of rock velocities encountered in the upper oceanic crust of oceanic plateaus [*Walther*, 2003]. In this hypothesis, OWB and IWB1 would belong to different petrologic domains of an oceanic plateau, and the deepest part of OWB, equivalent to IWB2 (Figure 3c), would have been removed, likely by subduction erosion.

[30] It is probable that the trailing flank of the Gorgona terrane was heavily eroded by subduction, so that progressively more internal zones of the margin basement were put into contact with the subduction fault. This contact may have favored fluids migration and tectonic shearing along splay faults. Fluids emanating at the seafloor in subduction zones are inferred to have migrated along deep crustal faults and have formed under temperatures of 85–150°C [*Hensen et al.*, 2004]. *Ranero et al.* [2008] present a set of convincing observations from offshore Nicaragua and Costa Rica indicating that at erosional margins, fluids drain from the plate boundary through the fractured upper plate to seep at the seafloor, rather than along the décollement. *Park et al.* [2002a] also suggest elevated fluid pressure along a Nankai splay fault on the basis of the reverse polarity reflection of the fault. Similarly, fluids derived from the SC are expected to flow along SF1 as suggested by the high-amplitude splay faults reflectivity of negative polarity shown in Figure 5. Although, no direct observation is available yet to document fluid seeps or mud volcanoes in our study area, migrating fluids are expected to contribute to basement rock alteration, particularly in the proximity of SF1, as indicated by the landward dipping, low-velocity zone sandwiched between IWB and the high-velocity core of OWB (Figure 3b).

[31] Both outer and inner wedge basement rocks, which are inferred oceanic, possibly include ultramafic rocks like the serpentinized peridotites reported on the nearby Gorgona Island [*Dietrich et al.*, 1981]. In this hypothesis, ultramafic rocks-fluids interaction would have led to partial serpentinization thus reducing locally rocks velocities and strength. Serpentinite has a relatively low density compared to overlying rocks [*Coleman*, 1971], so that the splay fault could provide the pathway for a diapiric rise of serpentinite, and account for the relatively low-velocity zone (3.5–3.8 km/s) located immediately beneath the summit graben and associated with SF1 (Figure 3b, km 25–30).

[32] Serpentinite may affect the mechanics of both SF1 and the updip segment of the interplate fault. At shallow depths and temperatures of 50–200°C, serpentine minerals as lizardite and antigorite are relatively strong, and can slip either unstably or stably depending on temperature-pressure-velocity conditions [*Moore et al.*, 1997]. A serpentinite bearing fault could easily propagate coseismic slip initiated deeper because serpentinite is velocity weakening at high-slip velocity [*Reinen et al.*, 1991]. Conversely, at shallow depths and low to moderate slip velocities, serpentinite has a velocity strengthening behavior [*Moore et al.*, 1997]. Thus, assuming that SF1 bears some serpentinite, this rock could favor coseismic slip propagation along the deeper segment of SF1, and contribute to slip damping along its upper segment. In addition to clays and high-porosity sediment entrained in the SC, velocity-strengthening behavior along the upper segment of the plate interface may result from the presence of serpentinite or talc-bearing serpentinite as recently discovered from the drilling of the creeping segment of the San Andreas Fault [*Moore and Rymer*, 2007]. Talc, which results from the reaction of serpentine minerals with Si-saturated fluids that migrate up the fault zone, has a very low shear strength compared to serpentine minerals [*Moore and Rymer*, 2007]. Laboratory tests show that talc resists to movement when sliding velocity is increased thus favoring slow, stable creep, inhibiting elastic stress buildup in the rock volume around the fault [*Wibberley*, 2007]. Talc could be an alternative to high-fluid pressure to account for the globally aseismic behavior of the upper segment of the plate interface along line SIS-44.

5.5.2. Margin Intrabasement Structures

[33] Intrabasement faults interpreted on line SIS-44 include a listric, normal fault that roots on a strong, subhorizontal reflector near a 16-km depth. Although the southeast, deepest corner of the velocity model is poorly controlled (Figure 3b), the subhorizontal reflector may be indicative of the continental Moho. However, on the basis of an onshore-offshore wide-angle seismic experiment from *Meissnar et al.* [1976], *Kellogg and Vega* [1995] constructed a density model with a continental Moho at a ~28-km depth beneath the marine part of the margin. Alternatively, the subhorizontal reflector is interpreted as the downward flattening segment of listric normal faults, and may represent an intracrustal detachment level (Figure 3b). This interpretation implies that the Cretaceous-Paleocene mafic basement of the margin was extensionally deformed. Basement reverse faults and folds located between km 39 and 49 show similar dips and shapes as the listric fault suggesting that normal faults were locally reactivated by compression.

[34] The strike-slip fault zone also provides strong evidence for crustal extension followed by transpression. The rift structure (Figure 6) may have filled up with flat-laying lavas, possibly intercalated with sediments, as suggested by its 3.0–4.8 km/s velocities (Table 1 and Figure 3b), prior to its inversion by transpression. This rift structure, which is about 20 km wide, can be closely related to the setting of the mafic igneous rocks that form fault blocks on Gorgona Island, and include flat-lying komatiite flows inter layered with basaltic flows [*Dietrich et al.*, 1981; *Kerr*, 2005]. *Storey et al.* [1991] proposed that Gorgona Island rocks are a part of a large Pacific-derived oceanic plateau. Therefore, we suggest that hot mantle plume-derived Gorgona rocks [*Kerr*, 2005] could have been emplaced in a rift zone at a divergent plate boundary structurally similar to that identified in northern Iceland [*Brandsdóttir et al.*, 1997]. Jumps of the rift axis may have allowed preservation of a rift structure as that identified in line SIS-44.

5.5.3. Timing of Deformation

[35] The intrabasement fault pattern represents a cumulative picture over time, which recorded extension and likely subsidence of the Gorgona terrane, prior to its oblique collision against South America and development of the present-day subduction. Stratigraphic correlations between seismic units of the fore-arc basin and onshore geology [*Marcaillou and Collot*, 2008] allow refining the periods of tectonic deformation, and better constrain the origin of the present-day splay faults.

[36] The 86–89 Ma old, mafic basement (unit F) [*Aitken and Echeverría*, 1984; *Sinton et al.*, 1998] deformed by normal faulting and truncated by the prominent Paleocene–

early Eocene unconformity (U5 in Figures 5 and 6) is good evidence for extensional tectonism of the Gorgona terrane to have occurred sometime during the latest Cretaceous and/or Paleocene. Upper Eocene sediment that crop out on Gorgonilla Island (Figure 2) are deformed and consist of limestone, pyroclastic rocks and deep water radiolarian shale deposited on mafic basement [*Dietrich et al.*, 1981] suggesting that Gorgona terrane suffered tectonic deformation during or after the late Eocene [*Kerr*, 2005]. The seismic facies analysis of units A–E and the stratigraphic correlation of these units with onshore geology imply that unit E consists of pre-late Eocene sediment and terminates by a latest Eocene-basal Oligocene unconformity (U4 in Figure 6) [*Marcaillou and Collot*, 2008]. Hence, the transpressive faulting that deformed unit E is compatible with dextral-oblique deformation of the Gorgona terrane during the Eocene or at the Eocene-Oligocene boundary. Strike-slip deformation has been a significant tectonics component of the Ecuador, Colombia margin, mainly during terrane accretion periods [*Daly*, 1989], as indicated by the SSFZ in line SIS-44 but also by other flower structures such as the one interpreted from MCS data to cut the offshore oceanic basement of central Ecuador near latitude 0°30 S [*Collot et al.*, 2004, Figure 4]. This later fault correlates with the major, onshore dextral Jama-Quininde strike-slip fault that according to *Deniaud* [2000] deformed later Cretaceous to lower Miocene sediment.

[37] On Gorgonilla Island, lower Oligocene to upper Miocene sediment includes siliceous silty shale and conglomerate with mafic elements [*Dietrich et al.*, 1981]. Unit D likely deposited during the Oligocene over unconformity U4, was locally strongly folded, as shown by MCS line SIS-45 adjacent to line SIS-44 [*Marcaillou and Collot*, 2008]. According to these authors, compression of unit D terminated by unconformity U3 inferred to be latest Oligocene–basal Miocene. This tectonic phase was followed by deposition of unit C and later compression that peaked during the middle Miocene with unconformity U2. This scenario, in which Eocene transpressive tectonics preceded more compressive Oligocene-Neogene deformation, is in good agreement with the remarkable changes in convergence direction and rate of the Farallon/Nazca plate relative to South America from rapid, dextral-oblique convergence throughout most of the Eocene to slower and less oblique since the latest Eocene as documented by *Pardo-Casas and Molnar* [1987] and *Daly* [1989].

5.5.4. Structural Implications

[38] The Cretaceous to Paleogene tectonic history of the Gorgona terrane shows clear implications for the development of splay faults, their potential role in outer wedge rock alteration, and their control on earthquake rupture zones. Splay fault 1 mimics the large intrabasement listric normal faults suggesting the splay fault initiated from them. The spoon shape of the listric normal faults provides a favorable geometry for thrust activation or fault slip inversion in a compressive stress field [*Cohen*, 1982], thus favoring development of subduction-related splay faults. Therefore, splay fault 1 is interpreted as a slip-inverted preexisting listric normal fault within the igneous basement. In this scenario, fluids migration along the fault was boosted when the listric normal fault connected to the plate interface, as a result of enduring subduction erosion (Figures 7a and 7b). In the context of a destructive margin, the flower structure in Figure 6, which is presently high-angle, inactive and disconnected with the plate interface, will tilt seaward and be put in contact with the interplate fault as a result of basal subduction erosion (Figure 7c), thus offering a favorable geometry to compressive fault reactivation, fluid circulation, rock alteration and earthquake rupture propagation.

6. Conclusions

[39] The analysis of a prestack depth migration (PSDM), multichannel seismic reflection section and associated velocity model reveals the structures of the north Ecuador–south Colombia subduction margin, and the potential origin of a major splay fault, which likely controlled the Mw 7.7, 1958 earthquake coseismic slip.

[40] 1. In the trench, the Nazca oceanic crust entering the subduction zone includes a 1.0- to 1.5-km-deep, rock-filled graben buried beneath a 3-km-thick trench fill associated with the Esmeraldas deep-sea turbidite system. Subduction of a 2-km-high buried seamount has no clear morphologic expression on the margin, but it forced the décollement thrust to rise upward and prevented frontal tectonic accretion. We speculate that similar features embedded in subducting sediment may be responsible for the 1958 earthquake maximum slip asperity.

[41] 2. The margin consists of a largely stable inner wedge overlain by a subhorizontal 2- to 3-km-thick forearc basin and an outer wedge characterized by a steep surface slope. Basal tectonic erosion of the outer margin wedge is supported by the trenchward tilt of the most seaward part of the fore-arc basin.

[42] 3. Slightly inboard of the trench slope break, the margin basement is cut by a steeply seaward rising (up to 33°) splay fault, which separates high-velocity (5–6.6 km/s) oceanic rocks of the inner wedge basement from 4 to 5 km/s outer wedge oceanic rocks, expected to be locally altered by SC-derived fluids.

[43] 4. On the basis of seismic reflectivity, the SC and interplate fault divide into three segments: (1) the shallowest one down to a 6-km depth dips 14° and truncates incoming trench fill; (2) the intermediate one between 6- and 9-km depths which is poorly reflective and dips 11° with an estimated ∼1.3-km maximum thickness and low velocity (according to the model proposed by *Wang and Hu* [2006], these interplate fault segments form the weak aseismic décollement thrust which will briefly become stronger during ruptures, and be activated in postseismic periods); and (3) the deep segment of the SC, between 9- and 15-km depths which is highly reflective, dips 11° and is roofed by the deep part of the splay fault, which is interpreted as the updip portion of the seismogenic zone. This segment is interpreted to be strong, and becomes weak during ruptures.

[44] 5. Because serpentinized ultramafic rocks are expected within the margin basement, serpentine minerals may control, at least partially, the rupture mechanics of the splay fault and interplate fault. In particular, talc may be an important cause of the slip strengthening behavior of the aseismic upper segment of the plate interface.

[45] 6. On the basis of seismic interpretation, we propose the formation of seaward dipping duplexes within the deep segment of the SC by underplating horses detached from the

subducting mélange over multiple earthquake cycles. Duplexes would form between the overlapping seismogenic splay fault–interplate fault and the underlying aseismic décollement thrust.

[46] 7. We identified fossil, margin intrabasement listric normal faults, and a shallow basement rift zone inverted in a positive flower structure. These structures likely resulted from various stages of the Gorgona terrane structural development and its oblique tectonic deformation against South America. The splay fault could have resulted from tectonic inversion of an ancient listric normal fault.

[47] 8. Profile SIS-44 shows evidence for both underplating and basal erosion, two conflicting processes that contribute to the growth or destruction of continental margins. Because the outer wedge rocks are severely eroded, the mass budget of the margin is locally negative and subsequently, underplating appears as a transient process along this segment of the north Ecuador–south Colombia margin.

Appendix A: Multichannel Seismic Reflection (MCS) and Wide-Angle Reflection/Refraction (WA) Data Acquisition and Processing

A1. Acquisition

[48] The 2-D MCS data acquisition was during the SISTEUR cruise on board the R/V *Nadir*. Streamer is 4.5 km long, has 348 groups at 12.5-m interval, recording 4-ms samples, with a 15-s record length. Source is a 48-L (2869 inch^3) air gun array tuned in a single-bubble mode and fired at 50-m interval. The geometry yielded a 43-fold MCS data set. OBS data acquisition was during the SALIERI cruise on board the R/V *Sonne*. Fourteen ocean bottom hydrophones (OBH) are from GEOMAR (Kiel, Germany). Ten four-component ocean bottom seismometers (OBS) are from Geosciences Azur (Villefranche-sur-Mer, France). Sources are three 32-L (5816 inch^3) air guns, with average shot spacing of 140 m.

A2. Preprocessing of MCS and WA Data

[49] MCS data were preprocessed using the Geovecteur software to prepare data for PSDM, preserving the amplitude of the data. Preprocessing included sorting of data to 6.25-m CDP, first pass velocity analysis, amplitudes attenuation (0.001 factor) of noisy traces, a band pass filter (3, 6, 50, 60 Hz), minimum phase operator, multiple attenuation in the frequency–wave number (FK) domain, normal move out velocity analysis, loose external mute, spherical divergence correction, predictive deconvolution, second multiple attenuation using Radon transform, inverse spherical divergence correction and inverse NMO correction, second bandpass filter (3, 6, 50, 60 Hz), and sorting of CDP to shot gather.

[50] Although WA data quality is variable, it is generally good with some arrivals being clearly identified at 120-km offsets in some record sections [*Gailler et al.*, 2007]. Processing consisted in correcting for clock drift during deployment and inverting the direct arrivals to obtain the instrument location and orientation (OBS). Further processing included the application of a Butterworth filter (low cut of 5 Hz, high cut of 15 Hz), predictive deconvolution (whitening) and amplitude equalization.

### A3. Prestack Depth Migration and Velocity Model Construction

[51] To obtain an optimal depth-migrated image, and a refined velocity model (see Figure 3), a four-step processing workflow based on a combination of velocities derived from MCS and coincident WA reflection and refraction data was designed.

[52] 1. MCS data are used to calculate an initial velocity model from NMO analysis. NMO velocities are converted to interval velocities using the Dix Equation. A 2-D model is interpolated from the internal velocity-depth function and subsequently smoothed for prestack depth migration in angle domain [*Thierry et al.*, 1999]. To correct a velocity model based on prestack depth migration, we implemented the method of migration velocity analysis proposed by *Al-Yahya* [1989]. As a result we obtained an accurate velocity model (v_mcs) and corresponding PSDM image for the shallow part of the section. Velocity estimations based on the curvature of reflectors in common image gathers (CIG) were poorly constrained for depths greater than the maximum offset of the streamer (4.5 km).

[53] 2. Wide-angle seismic data recorded by the OBS was used to perform the inversion of the first arrival travel times and obtain a large-scale velocity model [*Gailler et al.*, 2007]. This model (v_wa) contains velocity information for deeper levels than the velocity model derived from MCS data.

[54] 3. We built a mixed velocity model composed of three zones: (1) a shallow area, which contains the velocity information derived from MCS data (v_mcs) (the thickness of this region is estimated from the CIG and corresponds to the depth of the MCS velocity model), (2) a transition area, where a weighted average between both models (v_mcs and v_wa) is considered (the thickness of this area was estimated so that no discontinuity is generated within the velocity model), and (3) a deep zone, which contains only the velocity information derived from wide-angle data (v_wa) (this mixed velocity model is used to improve the prestack depth-migrated image). The plot of the final PSDM image included a depth variant automatic gain control (AGC) of amplitudes. Quality control and the accuracy of the migrated image is qualitatively controlled and quantitatively computed by CIG analysis and semblance estimation.

[55] 4. The mixed velocity macromodel is a smooth function. Therefore, reflected arrivals are modeled to define reflectors that simulate discontinuities in the modeled media. One way to include these reflectors is the construction of a blocky model. We used the parameterization of *Zelt and Smith* [1992] that divides each layer in trapeziums whose corners are nodes that define either the interface geometry or velocity. Velocity within each trapezium is a bilinear interpolation of the values in the velocity nodes placed at its corners. In the resulting blocky model, four kinds of observed times are modeled for each layer and their interfaces: (1) short offset reflections, generally displayed in CDP or CIG common image gathers, where MCS based velocity information can be obtained, (2) zero offset reflections, commonly presented in the stacked time section, provide
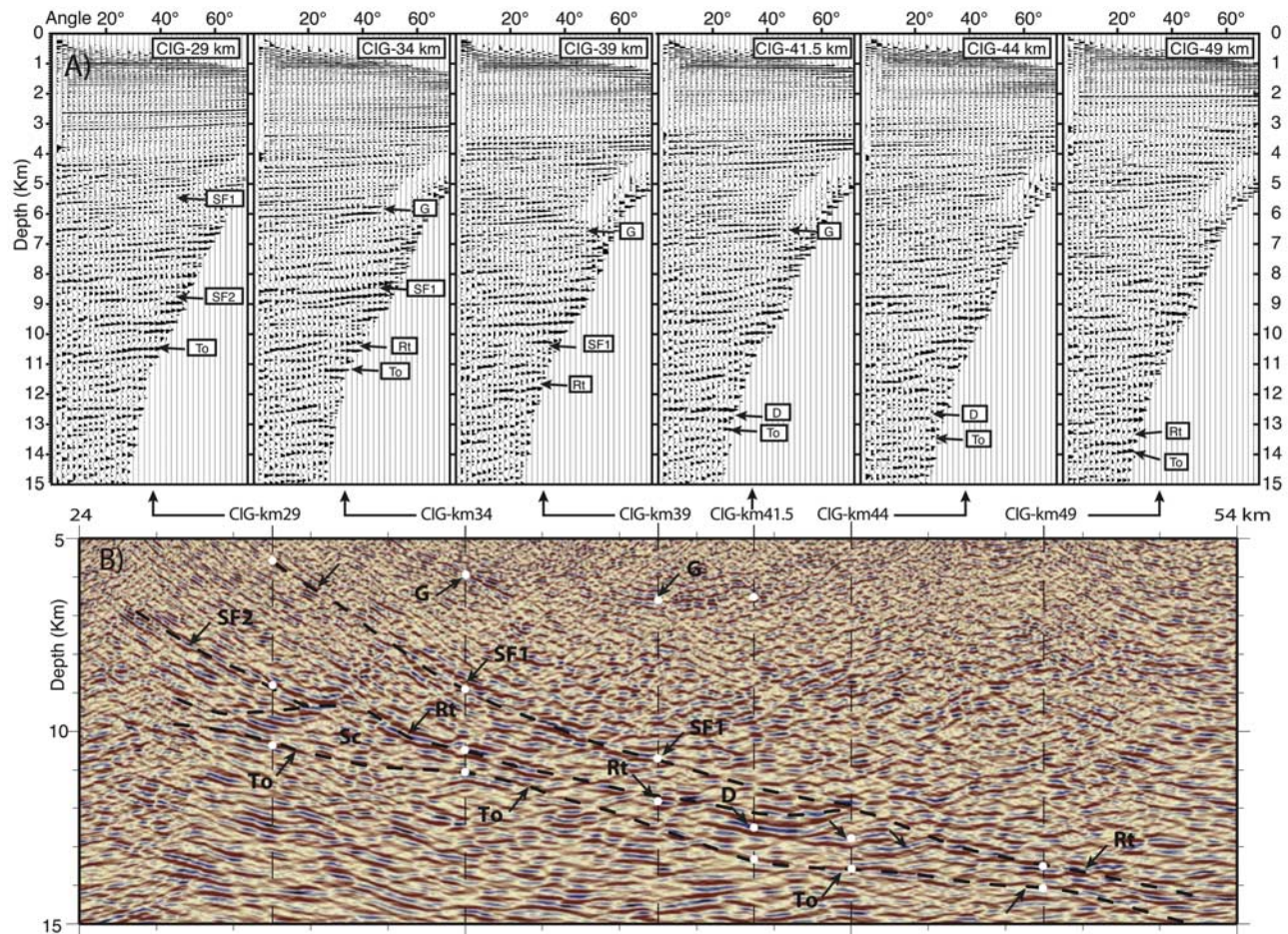
Figure B1. (a) IsoX panels (CIGs) obtained with the mixed velocity model along line SIS-44. (b) Location of IsoX panels shown in Figure B1a on part of the depth-migrated image of line SIS-44. Black and red are positive seismic polarity; white and blue are negative on Figures B1a and B1b, respectively. Reflections, as splay fault 1 (SF1), splay fault 2 (SF2), duplex (D), roof thrust (Rt), top of oceanic crust (To), and a margin internal reflector (G), are flat and coherent, indicating that the seismic reflectors are confidently imaged.

normal incidence travel time information, (3) wide-angle reflections, and (4) refractions (or first arrivals) travel times displayed in wide-angle record sections.

[56] Transformation from a smooth to a blocky model follows four steps: (1) main reflectors in the time-migrated image are picked, defining the geometry of the layer interfaces, (2) initial velocities for each layer are sampled from the smooth mixed velocity macromodel, (3) wide-angle and zero-offset synthetic travel times are computed and compared with those observed, and (4) velocity and geometry of each layer are inverted to minimize the misfit between observed and synthetic travel times (RSTTI package [*Operto*, 1996]). To assess the accuracy of the optimal velocity model, wide-angle refractions are estimated and compared with picked travel times from observed OBS data. In this way a velocity model that explains all the four kinds of arrivals is obtained.

Appendix B: IsoX (CIG) Panels

[57] IsoX panels are common image gathers, noted as CIGs, and represent the traces sorted by angle and extracted

from each partial seismic image at a given x coordinate (Figure B1). A partial image is a collection of diffracting points, which are illuminated under different angles. A continuous reflector is treated as a line of diffracting points, and the stack of all diffracting points over all angles forms the reflector image [*Thierry et al.*, 1999]. Inaccuracies of the velocity macromodel used for PSDM migration curve the reflector on CIGs. The velocity macromodel is iteratively corrected during migration until CIG are flattened. When this condition is satisfied, CIG are stacked to get the final migrated image.

References

Agudelo, W. (2005), Imagerie sismique quantitative de la marge convergente d'Equateur-Colombie, Ph.D. thesis, Univ. Pierre et Marie Curie, Paris.

Agudelo, W., A. Ribodetti, S. Operto, and A. Gailler (2004), Imaging deep reflectors: Combination of MCS and wide-angle data for a better estimation of the velocity macro-model, paper presented at 66th EAGE Conference, Eur. Assoc. of Geosci. Eng., Paris, France.

Aitken, B. G., and L. M. Echeverría (1984), Petrology and geochemistry of komatiites and tholeiites from Gorgona island, Colombia, *Contrib. Mineral. Petrol.*, 86, 94–105, doi:10.1007/BF00373714.

Allen, P. A., and J. R. Allen (1993), Basins associated with strike-slip deformation, in *Basin Analysis: Principles and Applications*, pp. 115–138, Blackwell Sci., Oxford, U.K.

Al-Yahya, K. (1989), Velocity analysis by iterative profile migration, *Geophysics*, 54, 718–729, doi:10.1190/1.1442699.

Bangs, N., T. H. Shipley, S. P. S. Gulick, G. F. Moore, S. Kuromoto, and Y. Nakamura (2004), Evolution of the Nankai Trough décollement from the trench into the seismogenic zone: Inferences from three-dimensional seismic reflection imaging, *Geology*, 32(4), 273–276, doi:10.1130/G20211.2.

Bangs, N. L. B., S. P. S. Gulick, and T. H. Shipley (2006), Seamount subduction erosion in the Nankai Trough and its potential impact on the seismogenic zone, *Geology*, 34(8), 701–704, doi:10.1130/G22451.1.

Beck, S. L., and L. J. Ruff (1984), The rupture process of the great 1979 Colombia earthquake: Evidence for the asperity model, *J. Geophys. Res.*, 89, 9281–9291, doi:10.1029/JB089iB11p09281.

Behrmann, J. H. (1991), Conditions for hydrofracture and the fluid permeability of accretionary wedges, *Earth Planet. Sci. Lett.*, 107, 550–558, doi:10.1016/0012-821X(91)90100-V.

Boyer, S. E., and D. Elliott (1982), Thrust systems, *AAPG Bull*, 66(9), 1196–1230.

Brandsdóttir, B., W. Menke, P. Einarsson, R. S. White, and R. K. Staples (1997), Färoe-Iceland Ridge experiment: 2. Crustal structure of the Krafla central volcano, *J. Geophys. Res.*, 102, 7867–7886, doi:10.1029/96JB03799.

Byrne, D. E., D. M. Davis, and L. R. Sykes (1988), Loci and maximum size of thrust earthquakes and the mechanics of the shallow region of subduction zones, *Tectonics*, 7(4), 833–857, doi:10.1029/TC007i004p00833.

Calahorrano, A., S. Sallares, J.-Y. Collot, F. Sage, and C. R. Ranero (2008), Nonlinear variations of the physical properties along the southern Ecuador subduction channel: Results from depth-migrated seismic data, *Earth Planet. Sci. Lett.*, 267(3–4), 453–467, doi:10.1016/j.epsl.2007.11.061.

Caress, D. W., M. K. McNutt, R. S. Detrick, and J. C. Mutter (1995), Seismic imaging of hotspot-related crustal underplating beneath the Marquesas Islands, *Nature*, 373, 600–603, doi:10.1038/373600a0.

Cediel, F., R. Shaw and P. C. Cáceres (2003), Tectonic assembly of the northern Andean Block, in *The Circum-Gulf of Mexico and the Caribbean: Hydrocarbon Habitats, Basin Formation, and Plate Tectonics*, edited by C. Bartolini, R. T. Buffler, and J. Blickwede, *AAPG Mem.*, 79, 815–848.

Charvis, P., A. Laesanpura, J. Gallart, A. Hirn, J.-C. Lépine, B. deVoogd, T. A. Minshull, Y. Hello, and B. Pontoise (1999), Spatial distribution of hotspot material added to the lithosphere under La Réunion, from wide-angle seismic data, *J. Geophys. Res.*, 104, 2875–2893, doi:10.1029/98JB02841.

Cloos, M. (1992), Thrust-type subduction-zone earthquakes and seamount asperities: A physical model for seismic rupture, *Geology*, 20(7), 601–604, doi:10.1130/0091-7613(1992)020<0601:TTSZEA>2.3.CO;2.

Cloos, M., and R. L. Shreve (1996), Shear-zone thickness and seismicity of Chilean- and Marianas-type subduction zones, *Geology*, 24(2), 107–110, doi:10.1130/0091-7613(1996)024<0107:SZTATS>2.3.CO;2.

Cohen, C. R. (1982), Model for a passive to active continental margin transition: Implications for hydrocarbure exploration, *AAPG Bull.*, 66(6), 708–718.

Coleman, R. G. (1971), Petrological and geophysical nature of serpentinites, *Geol. Soc. Am. Bull.*, 82, 897–918, doi:10.1130/0016-7606(1971)82[897:PAGNOS]2.0.CO;2.

Collot, J.-Y., and M. A. Fisher (1989), Formation of forearc basins by collision between seamounts and accretionary wedges: An example from the New Hebrides subduction zone, *Geology*, 17(10), 930–933, doi:10.1130/0091-7613(1989)017<0930:FOFBBC>2.3.CO;2.

Collot, J.-Y., S. Lallemand, B. Pelletier, J.-P. Eissen, G. Glaçon, M. A. Fisher, H. G. Greene, J. Boulin, J. Daniel, and M. Monzier (1992), Geology of the d'Entrecasteaux–New Hebrides Arc collision zone: Results from a deep submersible survey, *Tectonophysics*, 212, 213–241, doi:10.1016/0040-1951(92)90292-E.

Collot, J.-Y., B. Marcaillou, F. Sage, F. Michaud, W. Agudelo, P. Charvis, D. Graindorge, M.-A. Gutscher, and G. Spence (2004), Are rupture zone limits of great subduction earthquakes controlled by upper plate structures? Evidence from multichannel seismic reflection data acquired across the northern Ecuador–southwest Colombia margin, *J. Geophys. Res.*, 109, B11103, doi:10.1029/2004JB003060.

Collot, J.-Y., et al. (2005), Seafloor margin map helps in understanding subduction earthquakes, *Eos Trans. AGU*, 86(46), 464, doi:10.1029/2005EO460003.

Collot, J.-Y., F. Michaud, Y. Legonidec, A. Calahorrano, F. Sage, A. Alvarado, and Personal Científico y Técnico del INOCAR (2006), Mapas del margen continental Centro y Sur de Ecuador: Batimetría, Relieve, Reflectividad Acústica e Interpretación Geológica, *Publ. IOA-CVM-04-Post*, Inst. Oceanogr. de la Armada, Guayaquil, Ecuador.

Cummins, P. R., and Y. Kaneda (2000), Possible splay fault slip during the 1946 Nankai earthquake, *Geophys. Res. Lett.*, 27(17), 2725–2728, doi:10.1029/1999GL011139.

Cummins, P. R., T. Hori, and Y. Kaneda (2001), Splay fault and megathrust earthquake slip in the Nankai Trough, *Earth Planets Space*, 53, 243–248.

Daly, M. (1989), Correlations between Nazca/Farallon plate kinematics and forearc basin evolution in Ecuador, *Tectonics*, 8(4), 769–790, doi:10.1029/TC008i004p00769.

Deniaud, Y. (2000), Enregistrements sédimentaire et structural de l'évolution géodynamique des Andes Equatoriennes au cours du Néogène: Etude des bassins d'avant-arc et bilans de masse, Ph.D. thesis, Univ. Joseph Fourier, Grenoble, France.

Dietrich, V. J., A. Gansser, J. Sommerauer, and W. E. Cameron (1981), Palaeogene komatiites from Gorgona Island, East Pacific—A primary magma for ocean floor basalts?, *Geochem. J.*, 15, 141–161.

Dominguez, S., J. Malavieille, and S. Lallemand (2000), Deformation of margins in response to seamount subduction insights from sandbox experiments, *Tectonics*, 19(1), 182–196, doi:10.1029/1999TC900055.

Espinoza, J. (1992), Terremotos tsunamigenicos en el Ecuador, *Acta Oceanogr. Pac. INOCAR*, 7(1), 21–28.

Fisher, M. A., J. Y. Collot, and E. L. Geist (1991), Structures of the collision zone between Bougainville Guyot and the accretionary wedge of the New Hebrides Island Arc, southwest Pacific, *Tectonics*, 10(5), 887–903, doi:10.1029/91TC00860.

Fukao, Y. (1979), Tsunami earthquake and subduction processes near deep-sea trenches, *J. Geophys. Res.*, 84, 2301–2314.

Fuller, C. W., S. Willett, and M. T. Brandon (2006), Formation of fore-arc basins and their influence on subduction zone earthquakes, *Geology*, 34(2), 65–68, doi:10.1130/G21828.1.

Gailler, A., P. Charvis, and E. R. Flueh (2007), Segmentation of the Nazca and South American Plates along the Ecuador subduction zone from wide angle seismic profiles, *Earth Planet. Sci. Lett.*, 260, 444–464, doi:10.1016/j.epsl.2007.05.045.

Gansser, A. (1973), Facts and theories on the Andes, *J. Geol. Soc.*, 129, 93–131, doi:10.1144/gsjgs.129.2.0093.

Goosens, P. J., and W. I. Rose (1973), Chemical composition and age determination of tholeiitic rocks in the basic igneous complex, Ecuador, *Geol. Soc. Am. Bull.*, 84, 1043–1052, doi:10.1130/0016-7606(1973)84<1043:CCAADO>2.0.CO;2.

Harding, T. P. (1990), Identification of wrench faults using subsurface structural data: Criteria and pitfalls, *AAPG Bull.*, 74(10), 1590–1609.

Hardy, N. C. (1991), Tectonic evolution of the easternmost Panama Basin: Some new data and inferences, *J. South Am. Earth Sci.*, 4(3), 261–269, doi:10.1016/0895-9811(91)90035-J.

Hashimoto, Y., and G. Kimura (1999), Underplating process from mélange formation to duplexing: Example from the Cretaceous Shimanto Subbelt, Kii Peninsula, southwest Japan, *Tectonics*, 18(1), 92–107, doi:10.1029/1998TC900014.

Hensen, C., K. Wallmann, M. Schmidt, C. R. Ranero, and E. Suess (2004), Fluid expulsion related to mud extrusion off Costa Rica, A window to the subducting slab, *Geology*, 32(3), 201–204, doi:10.1130/G20119.1.

Henstock, T., L. C. McNeill, and D. R. Tappin (2006), Seafloor morphology of the Sumatran subduction zone: Surface rupture during megathrust earthquakes?, *Geology*, 34(6), 485–488, doi:10.1130/22426.1.

Husen, S., E. Kissling, and R. Quintero (2002), Tomographic evidence for a subducted seamount beneath the Gulf of Nicoya, Costa Rica: The cause of the 1990 Mw = 7.0 Gulf of Nicoya earthquake, *Geophys. Res. Lett.*, 29(8), 1238, doi:10.1029/2001GL014045.

Hyndman, R. D., and K. Wang (1995), The rupture zone of the Cascadia great earthquakes from current deformation and the thermal regime, *J. Geophys. Res.*, 100, 22,133–22,154, doi:10.1029/95JB01970.

Hyndman, R. D., K. Wang, and M. Yamano (1995), Thermal constraints on the seismogenic portion of the southwestern Japan subduction thrust, *J. Geophys. Res.*, 100, 15,373–15,392, doi:10.1029/95JB00153.

Hyndman, R. D., M. Yamano, and D. A. Oleskevich (1997), The seismogenic zone of subduction thrust faults, *Isl. Arc*, 6, 244–260, doi:10.1111/j.1440-1738.1997.tb00175.x.

Ikesawa, E. A., A. Sakaguchi, and G. Kimura (2003), Pseudotachylyte from an ancient accretionary complex: Evidence for melt generation during

seismic slip along a master décollement?, *Geology*, *31*(7), 637–640, doi:10.1130/0091-7613(2003)031<0637:PFAAAC>2.0.CO;2.

Ikesawa, E., G. Kimura, K. Sato, K. Ikehara, Y. Kitamura, A. Yamagushi, K. Ujiie, and Y. Hashimoto (2005), Tectonic incorporation of the upper part of the ocean crust to overriding plate of a convergent margin: An example for the cretaceous-early tertiary Mugi Melange, the Shimanto belt, Japan, *Tectonophysics*, *401*, 217–230, doi:10.1016/j.tecto.2005.01.005.

Jaillard, E., S. Benìtez, and G. H. Mascle (1997), Les déformations paléogènes de la zone d'avant-arc sud-équatorienne en relation avec l'évolution géodynamique, *Bull. Soc. Geol. Fr.*, *168*(4), 403–412.

Kanamori, H., and J. W. Given (1981), Use of long-period surface waves for rapid determination of earthquake-source parameters, *Phys. Earth Planet. Inter.*, *27*, 8–31, doi:10.1016/0031-9201(81)90083-2.

Kanamori, H., and K. C. McNally (1982), Variable rupture mode of the subduction zone along the Ecuador-Colombia coast, *Bull. Seismol. Soc. Am.*, *72*(4), 1241–1253.

Kato, T. (1983), High-angle reverse faulting associated with the 1946 Nankaido earthquake, *Tectonophysics*, *96*, 31–44, doi:10.1016/0040-1951(83)90242-1.

Kelleher, J. (1972), Rupture zones of large South American earthquakes and some predictions, *J. Geophys. Res.*, *77*, 2087–2103, doi:10.1029/JB077i011p02087.

Kellogg, J. N., and V. Vega (1995), Tectonic development of Panama, Costa Rica, and the Colombian Andes: Constraints from Global Positioning System geodetic studies and gravity, in *Geologic and Tectonic Development of the Caribbean Plate Boundary in Southern Central America*, edited by P. Mann, *Spec. Pap. Geol. Soc. Am.*, *295*, 75–86.

Kerr, A. C. (2005), La Isla de Gorgona, *Lithos*, *84*, 77–101.

Kerr, A. C., and J. Tarney (2005), Tectonic evolution of the Caribbean and northwestern South America: The case for accretion of two Late Cretaceous oceanic plateaus, *Geology*, *33*(4), 269–272, doi:10.1130/G21109.1.

Kimura, G., Y. Kitamura, Y. Hashimoto, A. Yamagushi, T. Shibata, K. Ujiie, and S. Okamoto (2007), Transition of accretionary wedge structures around the up-dip limit of the seismogenic subduction zone, *Earth Planet. Sci. Lett.*, *255*, 471–484, doi:10.1016/j.epsl.2007.01.005.

Kitamura, Y., et al. (2005), Mélange and its seismogenic roof décollement: A plate boundary fault rock in the subduction zone: An example from the Shimanto Belt, Japan, *Tectonics*, *24*, TC5012, doi:10.1029/2004TC001635.

Lay, T., H. Kanamori, and L. Ruff (1982), The asperity model and the nature of large subduction zone earthquakes, *Earthquake Predict. Res.*, *1*, 3–71.

Lebras, M., F. Mégard, C. Dupuy, and J. Dostal (1987), Geochemistry and tectonic setting of pre-collision Cretaceous and Paleogene volcanic rocks of Ecuador, *Geol. Soc. Am. Bull.*, *99*, 569–578, doi:10.1130/0016-7606(1987)99<569:GATSOP>2.0.CO;2.

Le Pichon, X., P. Henry, and S. Lallemant (1993), Accretion and erosion in subduction zones: The role of fluids, *Annu. Rev. Earth Planet. Sci.*, *21*, 307–331, doi:10.1146/annurev.ea.21.050193.001515.

Lonsdale, P. (1978), Ecuadorian Subduction System, *AAPG Bull*, *62*(12), 2454–2477.

Lonsdale, P. (2005), Creation of the Cocos and Nazca plates by fission of the Farallon plate, *Tectonophysics*, *404*, 237–264, doi:10.1016/j.tecto.2005.05.011.

Lonsdale, P., and K. D. Klitgord (1978), Structure and tectonic history of the eastern Panama Basin, *Geol. Soc. Am. Bull.*, *89*, 981–999, doi:10.1130/0016-7606(1978)89<981:SATHOT>2.0.CO;2.

Luzieux, L. D. A., F. Heller, R. Spikings, C. F. Vallejo, and W. Winkler (2006), Origin and Cretaceous tectonic history of the coastal Ecuadorian forearc between 1°N and 3°S: Paleomagnetic, radiometric and fossil evidence, *Earth Planet. Sci. Lett.*, *249*, 400–414, doi:10.1016/j.epsl.2006.07.008.

Marcaillou, B. (2003), Régimes tectoniques et thermiques de la marge Nord Equateur–Sud Colombie (0°–3.5°N): Implications sur la sismogenèse, Ph.D. thesis, Univ. Pierre and Marie Curie, Paris.

Marcaillou, B., and J.-Y. Collot (2008), Chronostratigraphy and tectonic deformation of the north Ecuador–south Colombian fore-arc basin, *Mar. Geol.*, *255*(1–2), 30–44.

Marcaillou, B., G. Spence, J.-Y. Collot, and K. Wang (2006), Thermal regime from bottom simulating reflectors along the north Ecuador–south Colombia margin: Relation to margin segmentation and great subduction earthquakes, *J. Geophys. Res.*, *111*, B12407, doi:10.1029/2005JB004239.

Masson, D. G., L. M. Parson, J. Milsom, G. Nichols, N. Sikumbang, B. Dwiyanto, and H. Kallagher (1990), Subduction of seamounts at the Java Trench: A view with long-range sidescan sonar, *Tectonophysics*, *185*, 51–65, doi:10.1016/0040-1951(90)90404-V.

McGeary, S., and Z. Ben-Avraham (1986), The accretion of Gorgona Island, Colombia: Multichannel seismic evidence, in *Tectonostratigraphic Terranes of the Circum-Pacific Region*, Earth Sci. Ser., vol. 1, edited by

D. G. Howell, pp. 543–554, Circum-Pac. Counc. for Energy and Miner. Resour., Houston, Tex.

Meissnar, R. O., E. R. Flueh, F. Stibane, and E. Berg (1976), Dynamics of the active plate boundary in southwest Colombia according to recent geophysical measurements, *Tectonophysics*, *35*, 115–136, doi:10.1016/0040-1951(76)90032-9.

Mendoza, C., and J. W. Dewey (1984), Seismicity associated with the great Colombia-Ecuador earthquakes of 1942, 1958 and 1979: Implications for barrier models of earthquake rupture, *Bull. Seismol. Soc. Am.*, *74*(2), 577–593.

Moore, D. E., and M. J. Rymer (2007), Talc-bearing serpentinite and the creeping section of the San Andreas fault, *Nature*, *448*, 795–797, doi:10.1038/nature06064.

Moore, D. E., D. A. Lockner, M. Shengi, R. Summers, and J. D. Byerlee (1997), Strengths of serpentinite gouges at elevated temperatures, *J. Geophys. Res.*, *102*(B7), 14,787–14,801, doi:10.1029/97JB00995.

Moore, G. F., N. L. Bangs, A. Taira, S. Kuramoto, E. Pangborn, and H. J. Tobin (2007), Three-dimensional splay fault geometry and implications for tsunami generation, *Science*, *318*, 1128–1131, doi:10.1126/science.1147195.

Moore, J. C., and D. Saffer (2001), Up-dip limit of the seismogenic zone beneath the accretionary prism of southwest Japan: An effect of diagenetic to low-grade metamorphic processes and increasing effective stress, *Geology*, *29*(2), 183–186, doi:10.1130/0091-7613(2001)029<0183:ULOTSZ>2.0.CO;2.

Mountney, N. P., and G. K. Westbrook (1997), Quantitative analysis of Miocene to recent forearc basin evolution along the Colombian margin, *Basin Res.*, *9*, 177–196, doi:10.1046/j.1365-2117.1997.00040.x.

Mukoyoshi, H., A. Sakaguchi, K. Otsuki, T. Hirono, and W. Soh (2006), Co-seismic frictional melting along an out-of-sequence thrust in the Shimanto accretionary complex. Implications on the tsunamigenic potential of splay fault in modern subduction zones, *Earth Planet. Sci. Lett.*, *245*, 330–343.

Operto, S. (1996), RSTTI package: Ray based seismic travel time inversion, in *Tech. Rep. 148*, edited by Univ. of Tex. Inst. for Geophys., Austin.

Pardo-Casas, F., and P. Molnar (1987), Relative motion of the Nazca (Farallon) and South America plates since Late Cretaceous time, *Tectonics*, *6*(3), 233–248, doi:10.1029/TC006i003p00233.

Park, J.-O., T. Tsuru, S. Kodaira, A. Nakanishi, S. Miura, Y. Kaneda, and Y. Kono (2000), Out-of-sequence thrust faults developed in the co-seismic slip zone of the 1946 Nankai earthquake (Mw = 8.2) off Shikoku, southwest Japan, *Geophys. Res. Lett.*, *27*(7), 1033–1036, doi:10.1029/1999GL008443.

Park, J.-O., T. Tsuru, S. Kodaira, P. R. Cummins, and Y. Kaneda (2002a), Splay fault branching along the Nankai subduction zone, *Science*, *297*, 1157–1160, doi:10.1126/science.1074111.

Park, J., T. Tsuru, N. Takahashi, T. Hori, S. Kodaira, A. Nakanishi, S. Miura, and Y. Kaneda (2002b), A deep strong reflector in the Nankai accretionary wedge from multichannel seismic data: Implications for underplating and interseismic shear stress release, *J. Geophys. Res.*, *107*(B4), 2061, doi:10.1029/2001JB000262.

Plafker, G. (1972), Alaskan earthquake of 1964 and Chilean earthquake of 1960: Implications for arc tectonic, *J. Geophys. Res.*, *77*, 901–925, doi:10.1029/JB077i005p00901.

Ranero, C. R., and R. von Huene (2000), Subduction erosion along the Middle America convergent margin, *Nature*, *404*, 748–752, doi:10.1038/35008046.

Ranero, C. R., I. Grevemeyer, H. Sahling, U. Barckhausen, C. Hensen, K. Wallmann, W. Weinrebe, P. Vannucchi, R. von Huene, and K. McIntosh (2008), Hydrogeological system of erosional convergent margins and its influence on tectonics and interplate seismogenesis, *Geochem. Geophys. Geosyst.*, *9*, Q03S04, doi:10.1029/2007GC001679.

Ratzov, G., M. Sosson, J.-Y. Collot, S. Migeon, F. Michaud, E. Lopez, and Y. Le Gonidec (2007), Submarine landslides along the North Ecuador–South Colombia convergent margin. Possible tectonic control, in *Submarine Mass Movements and Their Consequences*, Adv. Nat. Technol. Hazards Res., vol. 27, edited by V. Lykousis, D. Sakellariou, and J. Locat, 47–55, Springer, New York.

Reinen, L. A., J. D. Weeks, and T. E. Tullis (1991), The frictional behavior of serpentinite: Implications for aseismic creep on shallow crustal faults, *Geophys. Res. Lett.*, *18*(10), 1921–1924.

Reynaud, C., E. Jaillard, H. Lapierre, M. Mamberti, and G. H. Mascle (1999), Oceanic plateau and island arcs of southwestern Ecuador: Their place in the geodynamic evolution of northwestern South America, *Tectonophysics*, *307*, 235–254, doi:10.1016/S0040-1951(99)00099-2.

Saffer, D., and C. Marone (2003), Comparison of smectite- and illite-rich gouge frictional properties: Application to the updip limit of the seismogenic zone along subduction megathrust, *Earth Planet. Sci. Lett.*, *215*, 219–235, doi:10.1016/S0012-821X(03)00424-2.

Sage, F., J.-Y. Collot, and C. R. Ranero (2006), Interplate patchiness and subduction-erosion mechanisms: Evidence from depth migrated seismic images at the central Ecuador convergent margin, *Geology*, *34*(12), 997–1000, doi:10.1130/G22790A.1.

Sallares, V., and P. Charvis (2003), Crustal thickness constraints on the geodynamic evolution of the Galapagos Volcanic Province, *Earth Planet. Sci. Lett.*, *214*, 545–559, doi:10.1016/S0012-821X(03)00373-X.

Sample, J. C., and D. M. Fisher (1986), Duplex accretion and underplating in an ancient accretionary complex, Kodiak Islands, Alaska, *Geology*, *14*, 160–163.

Scholl, D. W., R. von Huene, T. L. Vallier, and D. G. Howell (1980), Sedimentary masses and concepts about tectonic processes at underthrust ocean margins, *Geology*, *8*(12), 564–568, doi:10.1130/0091-7613(1980)8<564:SMACAT>2.0.CO;2.

Scholz, C. H. (1998), Earthquakes and friction laws, *Nature*, *391*, 37–42, doi:10.1038/34097.

Scholz, C. H., and C. Small (1997), The effect of seamount subduction on seismic coupling, *Geology*, *25*(6), 487–490, doi:10.1130/0091-7613(1997)025<0487:TEOSSO>2.3.CO;2.

Shipley, T. H., G. F. Moore, N. Bangs, J. C. Moore, and P. L. Stoffa (1994), Seismically inferred dilatancy distribution, northern Barbados Ridge décollement: Implications for fluid migration and fault strength, *Geology*, *22*(5), 411–414, doi:10.1130/0091-7613(1994)022<0411:SIDDNB>2.3.CO;2.

Shreve, R. L., and M. Cloos (1986), Dynamics of sediment subduction, melange formation, and prism accretion, *J. Geophys. Res.*, *91*, 10,229–10,245, doi:10.1029/JB091iB10p10229.

Sinton, C. W., R. A. Duncan, M. Storey, J. Lewis, and J. J. Estrada (1998), An oceanic flood basalt province within the Caribbean plate, *Earth Planet. Sci. Lett.*, *155*, 221–235, doi:10.1016/S0012-821X(97)00214-8.

Storey, M., J. J. Mahoney, L. W. Kroenke, and A. D. Saunders (1991), Are oceanic plateaus sites of komatiite formation?, *Geology*, *19*(4), 376–379, doi:10.1130/0091-7613(1991)019<0376:AOPSOK>2.3.CO;2.

Swenson, J. L., and S. L. Beck (1996), Historical 1942 Ecuador and 1942 Peru subduction earthquakes, and earthquake cycles along Colombia-Ecuador and Peru subduction segments, *Pure Appl. Geophys.*, *146*(1), 67–101, doi:10.1007/BF00876670.

Thierry, P., S. Operto, and G. Lambaré (1999), Fast 2-D ray+Born migration/inversion in complex media, *Geophysics*, *64*, 162–181, doi:10.1190/1.1444513.

Trenkamp, R., J. N. Kellogg, J. T. Freymueller, and H. P. Mora (2002), Wide plate margin deformation, southern Central America and northwestern South America, CASA GPS observations, *J. South Am. Earth Sci.*, *15*, 157–171, doi:10.1016/S0895-9811(02)00018-4.

Tsuru, T., J. Park, S. Miura, S. Kodaira, Y. Kido, and T. Hayashi (2002), Along-arc structural variation of the plate boundary at the Japan Trench margin: Implication of interplate coupling, *J. Geophys. Res.*, *107*(B12), 2357, doi:10.1029/2001JB001664.

von Huene, R., and S. Lallemand (1990), Tectonic erosion along the Japan and Peru convergent margins, *Geol. Soc. Am. Bull.*, *102*, 704–720, doi:10.1130/0016-7606(1990)102<0704:TEATJA>2.3.CO;2.

von Huene, R., C. R. Ranero, W. Weinrebe, and K. Hinz (2000), Quaternary convergent margin tectonics of Costa Rica, segmentation of the Cocos Plate and Central American volcanism, *Tectonics*, *19*(2), 314–334, doi:10.1029/1999TC001143.

von Huene, R., C. R. Ranero, and P. Vannucchi (2004), Generic model of subduction erosion, *Geology*, *32*(10), 913–916, doi:10.1130/G20563.1.

Walther, C. H. E. (2003), The crustal structure of the Cocos ridge off Costa Rica, *J. Geophys. Res.*, *108*(B3), 2136, doi:10.1029/2001JB000888.

Wang, K., and Y. Hu (2006), Accretionary prisms in subduction earthquake cycles: The theory of dynamic Coulomb wedge, *J. Geophys. Res.*, *111*, B06410, doi:10.1029/2005JB004094.

Wibberley, C. A. J. (2007), Talc at fault, *Nature*, *448*, 756–757, doi:10.1038/448756a.

Woodcock, N. H., and M. Fisher (1986), Strike-slip duplexes, *J. Struct. Geol.*, *8*(7), 725–735, doi:10.1016/0191-8141(86)90021-0.

Zelt, C. A., and R. B. Smith (1992), Seismic travel time inversion for 2-D crustal velocity structure, *Geophys. J. Int.*, *108*, 16–34, doi:10.1111/j.1365-246X.1992.tb00836.x.

_____

W. Agudelo, J.-Y. Collot, and A. Ribodetti, Geoscience Azur, Université de Nice-Sophia Antipolis, IRD, Université Pierre et Marie Curie, Observatoire de la Côte d'Azur, CNRS, BP 48, F-06235, Villefranche-sur-Mer, France. (collot@geoazur.obs-vlfr.fr)

B. Marcaillou, IFREE/JAMSTEC, 2.15 Natsushima-cho, Yokosuka, Kanagawa, 237-0061, Japan.